ESPOO 2008 VTT RESEARCH NOTES 2443

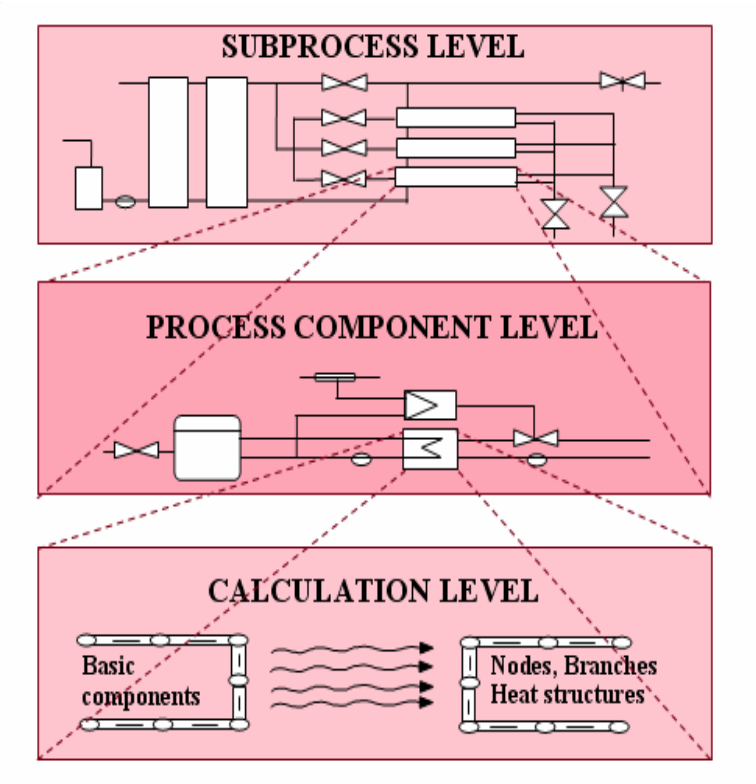

Markku Hänninen & Jukka Ylijoki

The one-dimensional separate two-phase flow model of APROS

VTT TIEDOTTEITA – RESEARCH NOTES 2443

The one-dimensional separate two-phase flow model of APROS

Markku Hänninen & Jukka Ylijoki

ISBN 978-951-38-7224-3 (soft back ed.)
ISSN 1235-0605 (soft back ed.)

ISBN 978-951-38-7225-0 (URL: http://www.vtt.fi/publications/index.jsp)
ISSN 1455-0865 (URL: http://www.vtt.fi/publications/index.jsp)

JULKAISIJA – UTGIVARE – PUBLISHER

VTT, Vuorimiehentie 5, PL 1000, 02044 VTT
puh. vaihde 020 722 111, faksi 020 722 7001

VTT, Bergsmansvägen 5, PB 1000, 02044 VTT
tel. växel 020 722 111, fax 020 722 7001

VTT Technical Research Centre of Finland, Vuorimiehentie 5, P.O. Box 1000, FI-02044 VTT, Finland
phone internat. +358 20 722 111, fax +358 20 722 7001

VTT, Tietotie 3, PL 1000, 02044 VTT
puh. vaihde 020 722 111, faksi 020 722 7012

VTT, Datavägen 3, PB 1000, 02044 VTT
tel. växel 020 722 111, fax 020 722 7012

VTT Technical Research Centre of Finland, Tietotie 3, P.O. Box 1000, FI-02044 VTT, Finland
phone internat. +358 20 722 111, fax +358 20 722 7012

Technical editing Anni Repo

Edita Prima Oy, Helsinki 2008

Hänninen, Markku & Ylijoki, Jukka. The one-dimensional separate two-phase flow model of APROS. Espoo 2008. VTT Tiedotteita – Research Notes 2443. 61 p.
Keywords thermal-hydraulics, two-phase flow, one-dimensional flow, heat transfer, boron concentration, non-condensable gas

Abstract

The publication describes the one-dimensional two-fluid model of the computer program APROS used for the simulation of nuclear and conventional power plants. The work is based on the technical report from 1992. The treatment of the non-condensable gas mass equation has been added. The test results have been updated, so that the results correspond to the present APROS version 5.08. The derivation of the model from the governing partial differential equations is shown in detail and the solution procedure is described. Correlations for interfacial and wall friction and for heat transfer have been used to close the set of the linear equations. The friction and heat transfer packages of the model are documented. Finally, results of test cases calculated with the present model are briefly discussed.

Preface

In the nuclear technology starting from 70's the safety analysis called for thermal-hydraulic models that were reliable enough to calculate the complex phenomena related to the normal and accident situations of the water cooled reactors. These codes were developed in many countries were the nuclear reactors were planed and were taken into use. In the USA several versions of the RELAP-codes were developed and gradually were improved by using more detailed physical description. In France the CATHARE code was developed and in Germany the code called ATHLET is used.

In Finland as a joint effort between VTT Technical Research Centre of Finland and Imatran Voima Oy the code APROS was developed. It is in many respects similar to many other thermal-hydraulic codes but already from the very beginning the aim was to develop the multipurpose code. Even if the APROS is capable to simulate the reactor thermal hydraulics it can be applied to many other processes because it includes also many other program packages than thermal hydraulics. Models for the automation system, the electrical system and for different plant components enable the simulation of whole power plants.

Even if the numerical calculation of the flows, enthalpies and pressures in APROS thermal hydraulic models is based on the finite difference scheme, the definition of the simulated process is made by using the process component modules. In addition the graphical interface called GRADES can be used for model construction, on-line modifications and control and monitoring of the simulation process. A code user can work on three different levels: process, process component and calculation levels. The typical process components used in APROS are pipes, pumps, valves and heat exchangers. Also process components specific for conventional or nuclear power plant can be used. At the same time when a user specifies the necessary data of a process component he defines how detailed the process component is to be simulated, i.e. how many finite difference elements are used in simulation. The APROS initialization program creates automatically the calculation nodalization on the basis of process components input data given by a user.

Contents

List of symbols

A	flow area (m^2)
a	matrix coefficient
C	boron concentration (ppm)
C	friction coefficient
C	relaxation coefficient
C	velocity of the disturbance wave (m/s)
c	heat capacity (J/kg°C)
D	hydraulic diameter of the flow channel (m)
E	rate of entrainment
F	friction force/volume (N/m^3)
F_η	viscosity number
G	mass flux (kg/m^2s)
g	acceleration of gravity (m/s^2)
Gr	Grashof number
h	height (m)
h	specific enthalpy (J/kg)
K	heat transfer coefficient (kg/m^3s)
L	bubble diameter (m)
p	pressure (Pa)
Pr	Prandtl number
Q	heat flux (W/m^2)
q	heat flow/volume (W/m^3)
Re	Reynolds number
S	source term
T	temperature (°C)
t	time (s)
u	velocity (m/s)
V	volume (m^3)
W	momentum flow (N)
X	mass fraction of gas phase
x	concentration
z	space coordinate (m)

Δz	length (m)
α	volume fraction of a phase
β	weighting factor
Γ	mass phase change rate (kg/m^{3}s)
Δh	enthalpy change (J/kg)
Δm	mass error (kg/s), mass source term (kg/s)
Δp	pressure loss or pressure change (Pa)
Δt	time step (s)
Δu	difference between phase velocities (m/s)
δ	droplet diameter (m)
η	dynamic viscosity (kg/m s)
χ	thermal conductivity (W/m°C)
π	dimensionless velocity
ρ	density (kg/m^3)
σ	surface tension (N/m)

Subscripts

a	annular flow
b	bubbly flow, boron
CHF	critical heat flux
cr	critical
d	droplet, droplet flow
fl	form loss
fr	frozen
g	gas phase
i	node i, interface
i-½	branch between nodes i-1 and i
i+½	branch between nodes i and i+1
i+3/2	branch between nodes i+1 and i+2
k	gas or liquid phase
l	liquid phase
max	maximum value

MFB	minimum film boiling
nc	non-condensable gas
p	constant pressure
pu	pump
qf	quench front
rad	radiation
sat	saturation
stat	static
v	valve
w	wall

Superscripts

n	new iteration step
n-1	previous iteration step
t-Δt	old time step

Special notations

max(*a,b*)	greater of *a* and *b*
min(*a,b*)	smaller of *a* and *b*
$\overline{\alpha}_{i+1/2}$	calculated as $\left(\alpha_i + \alpha_{i+1}\right)/2$
[*u*,0]	greater of *u* and 0

List of APROS variables

The variables beginning with TB are branch variables, node variables begin with TN, variables of heat transfer modules with H6 and heat structure node variables with HS.

Symbol	Variables	Description
A	TBAREA, TNAREA	flow area (m²)
A	HSAREA	area of heat transfer surface (m²)
C	TBKI	friction coefficient including the effect of valves and form loss (= $C_v + C_{fl}$)
C_{fl}	TBRKI	form loss coefficient
C_{fr}	TNCI	frozen velocity of the disturbance wave (m/s)
C_{wg}	TBFRCG	wall friction coefficient of gas
C_{wl}	TBFRCL	wall friction coefficient of liquid
c_{pg}	TNCPG	heat capacity of gas (J/kg°C)
c_{pl}	TNCPL	heat capacity of liquid (J/kg°C)
D	TBDI, TNDI	hydraulic diameter (m)
D_g	TBDGPS	term in the velocity equation of gas (m²s/kg): see formula (37)
D_l	TBDLPS	term in the velocity equation of liquid (m²s/kg): see formula (38)
E	TBENTR, TNENTR	rate of entrainment
e_g	TNCEG	term in the pressure equation (1/m s): see formula (63)
e_l	TNCEL	term in the pressure equation (1/m s): see formula (63)
F_i	TBFRI	interfacial friction (N/m^3)
F_{wg}	TBFRG	friction between wall and gas (N/m^3)
F_{wl}	TBFRL	friction between wall and liquid (N/m^3)
f_g	TNCFG	term in the pressure equation (kg/s): see formula (54)

f_l	TNCFL	term in the pressure equation (kg/s): see formula (54)
G	TNMFLU	mass flux of fluid (kg/m²s)
$\overline{g}$	TBGRAV	acceleration of gravity in the flow direction (m/s²)
h	TNLI, HSNLI	centre height in m (compared to a reference height)
h_g	TNHGT	specific enthalpy of gas (J/kg)
$h_{g,sat}$	TNHIPS	saturation enthalpy of gas (J/kg)
$h_{g,stat}$	TNHGS	static enthalpy of gas (J/kg)
h_{ig}	TNHGI	interface enthalpy of gas (J/kg)
h_{il}	TNHLI	interface enthalpy of liquid (J/kg)
h_l	TNHLT	specific enthalpy of liquid (J/kg)
$h_{l,sat}$	TNHIPW	saturation enthalpy of liquid (J/kg)
$h_{l,stat}$	TNHLS	static enthalpy of liquid (J/kg)
h_{qf}	TPZFT	height of the quench front (m)
K_{ig}	TNIHCG	interfacial heat transfer coefficient of gas (kg/m^{3}s)
K_{il}	TNIHCL	interfacial heat transfer coefficient of liquid (kg/m^{3}s)
M_g	TBMFLG	momentum flow of gas (N)
$M_{g,FL}$	TBDMFG	part of the change of momentum flow of gas (N): see Equations (43) and (44)
M_l	TBMFLL	momentum flow of liquid (N)
$M_{l,FL}$	TBDMFL	part of the change of momentum flow of liquid (N)
p	TNPI	pressure (Pa)
Pr_g	TNPRG	Prandtl number of gas
Pr_l	TNPRL	Prandtl number of liquid
Q_{cr}	H6HFCR	critical heat flux (W/m²)
$Q_{g,rad}$	H6HFRG	radiation heat flux between wall and gas (W/m²)
$Q_{l,rad}$	H6HFRL	radiation heat flux between wall and liquid (W/m²)
Q_{wg}	H6HFG	heat flux between wall and gas (without radiation, W/m²)
Q_{wi}	H6HFI	heat flux between wall and interface (without radiation, W/m²)
Q_{wl}	H6HFL	heat flux between wall and liquid (without radiation, W/m²)
q	HSQI	heat flow between wall and fluid (W)
q_{wg}	TNQIG	heat flow between wall and gas (W/m^3)
q_{wi}	TNQII	heat flow between wall and interface (W/m^3)

q_{wl}	TNQIL	heat flow between wall and liquid (W/m^3)
Re_d	TBRED, TNRED	Reynolds number of droplet
Re_g	TBREG	Reynolds number of gas
Re_l	TBREL, TNREL	Reynolds number of liquid
S_g	TNEGSO	energy source of gas (W): see formula (79)
S_l	TNELSO	energy source of liquid (W): see formula (79)
T_g	TNTG	temperature of gas (°C)
T_l	TNTL	temperature of liquid (°C)
T_{MFB}	H6TMFS	minimum film boiling temperature (°C)
T_{sat}	TNTSAT	saturation temperature of fluid (°C)
T_w	HSTW	wall temperature (°C)
U_g	TBUGPS	term in the velocity equation of gas (m/s): see formula (38)
U_l	TBULPS	term in the velocity equation of liquid (m/s): see formula (39)
u_g	TBUG, TNUG	velocity of gas (m/s)
u_l	TBUL, TNUL	velocity of gas (m/s)
V	TBVOL, TNVI	volume (m^3)
W	TBMAFL	mass flow of fluid (kg/s)
W_g	TBWGI	mass flow of gas (kg/s)
W_l	TBWLI	mass flow of liquid (kg/s)
x_b	TNBORI	boron concentration (ppm)
X	TNXST	mass fraction of gas phase
α	TBALFA, TNALFI	volume fraction of gas phase
$\alpha\rho_g$	TBAROG	upwind void fraction·density of gas (kg/m^3)
$\overline{\alpha\rho}_g$	TBARGA	average void fraction·density of gas (kg/m^3)

$(1-\alpha)\rho_l$	TBAROL	upwind void fraction·density of liquid (kg/m^3)
$\overline{(1-\alpha)\rho_1}$	TBARLA	average void fraction·density of liquid (kg/m^3)
Γ	TBGAM, TNGAM	phase change rate (kg/m^{3}s)
Δh_{gmax}	TNHMXG	maximum allowed change of gas enthalpy (J/kg)
Δh_{lmax}	TNHMXL	maximum allowed change of liquid enthalpy (J/kg)
Δm_g	TNMGER	mass error of gas in enthalpy solution (kg/s): see Equation (80)
$\Delta m_{g,i}$	TNMGSO	source term of gas mass in pressure solution (kg/s): see Equation (57)
$\Delta m_{l,i}$	TNMLER	mass error of liquid in enthalpy solution (kg/s): see Equation (80)
$\Delta m_{l,i}$	TNMLSO	mass source of liquid in pressure solution (kg/s): see Equation (57)
Δp_{pu}	TBHPUM	pressure loss of pump (Pa)
Δu	TBDU, TNDU	difference between velocities of gas and liquid (m/s)
Δz	TBLEN	length (m)
δ	TBDRDI, TNDRDI	droplet diameter (m)
η_g	TBDVG, TNDVG	dynamic viscosity of gas (kg/m s)
η_l	TBDVL, TNDVL	dynamic viscosity of liquid (kg/m s)
λ_g	TNLAG	thermal conductivity of gas (W/m°C)
λ_l	TNLAL	thermal conductivity of liquid (W/m°C)
ρ	TBRI, TNRI	density of fluid (kg/m^3)
ρ_g	TBRGI, TNRGI	density of gas (kg/m^3)
ρ_l	TBRLI, TNRLI	density of liquid (kg/m^3)
σ	TBSIGM, TNSIGM	surface tension (N/m)

$\partial F_g/\partial u_g$	TBDWDG	derivative of friction between wall and gas in respect to gas velocity (kg/m^{3}s)
$\partial F_i/\partial \Delta u$	TBDIDU	derivative of interfacial friction in respect to velocity difference (kg/m^{3}s)
$\partial F_l/\partial u_l$	TBDWDL	derivative of friction between wall and liquid in respect to liquid velocity (kg/m^{3}s)
$\partial T_w/\partial z$	HSDTDZ	wall temperature gradient in the flow direction (°C/m)
$\partial W/\partial u_g$	TBDMDG	derivative of fluid mass flow in respect to gas velocity (kg/m)
$\partial \Delta p_{pu}/\partial W$	TBDHPU	derivative of pump pressure loss in respect to fluid mass flow (1/m s): $\partial \Delta p_{pu}/\partial u_k = \partial \Delta p_{pu}/\partial W \cdot \partial W/\partial u_k$
$\partial \rho_g/\partial p$	TNDRPG	derivative of gas density in respect to pressure
$\partial \rho_l/\partial p$	TNDRPL	derivative of liquid density in respect to pressure

1. Introduction

APROS is a process simulator program originally developed by VTT Technical Research Centre of Finland and Imatran Voima Oy. Currently the program is co-developed and co-owned by VTT Technical Research Centre of Finland and Fortum Nuclear Services Ltd. The program is able to simulate dynamically thermal hydraulic processes in nuclear and conventional power plants.

In APROS process simulation code, the two-phase flow can be simulated with a various level of sophistication: with a homogeneous model, with a 5-equation drift-flux model and with a 6-equation two-fluid model. All the models can be used in the same simulation exercise, so that the parts of process simulated with one of the models can be connected to other parts simulated with different two-phase flow models. In the presented report the 6-equation part of the simulation system is described.

The separate one-dimensional two-phase flow model of APROS simulates the behavior of a system containing gas and liquid phases. The system is governed by six partial differential equations, from which pressures, void fractions and phase velocities and enthalpies are solved. The phases are coupled to each other with empirical friction and heat transfer terms which strongly affect the solution. The governing equations are discretized in respect with time and space and the resulting linear equation groups are solved by the equation solving system of APROS.

In the two-fluid model of APROS also the treatment of the non-condensable gases has been included. In the present model it is assumed that there is only one non-condensable gas present at a time in the simulated system. The simulated gases are air, nitrogen, helium and hydrogen.

In the model the non-condensable gas was assumed to stay in the gas phase, where the non-condensable gas and the steam form the homogeneous mixture, i.e. they have the same temperature and the same velocity.

In the present model also the non-condensable gas can be as a dissolved component in the liquid phase.

The two-phase flow model can be connected to the heat conduction solution of solid heat structures by calculating heat flows between the two systems. APROS contains several flow models of different accuracy levels. The results of other models can be given as boundary conditions to the two-phase model.

Pressures, void fractions and enthalpies are solved in the defined calculation control volumes (nodes). The velocities are calculated in control volumes between nodes (branches). One branch connects two adjacent nodes. The heat flows between the solid

heat structure and fluid are calculated in special heat transfer modules connecting the two systems. If different flow models are connected, connecting branches are defined between the nodes of the different accuracy levels and flows are calculated in the branches.

2. Governing equations

The calculation of the two-phase flow system is based on the conservation equations of mass, momentum and total energy of liquid and steam phases. If the gas includes also non-condensable gas the equation of the non-condensable gas is needed. The differential equations can be presented as follows /1/:

(mass of phases)
$$\frac{\partial \alpha_k \rho_k}{\partial t} + \frac{\partial \alpha_k \rho_k u_k}{\partial z} = \Gamma_k \tag{1}$$

(momentum of phases)
$$\frac{\partial \alpha_k \rho_k u_k}{\partial t} + \frac{\partial \alpha_k \rho_k u_k^2}{\partial z} + \alpha_k \frac{\partial p}{\partial z} = \Gamma_k u_{ik} + \alpha_k \rho_k \vec{g} + F_{wk} + F_{ik} + f_k(v, pu, fl) \tag{2}$$

(energy of phases)
$$\frac{\partial \alpha_k \rho_k h_k}{\partial t} + \frac{\partial \alpha_k \rho_k u_k h_k}{\partial z} = \alpha_k \frac{\partial p}{\partial t} + \Gamma_k h_{ik} + q_{ik} + q_{wk} + F_{ik} u_{ik} + \alpha_k \rho_k u_k \vec{g} \tag{3}$$

(mass of non-condensable gas)
$$\frac{\partial(\alpha_g \rho_{nc})}{\partial t} + \frac{\partial(\alpha_g \rho_{nc} u_g)}{\partial z} = 0 \tag{4}$$

In Equations (1) to (4) the subscript k refers to gas (g) or liquid (l) phases, i refers to the interface of the phases and w refers to the wall of a flow channel. The function f_k in the momentum equation takes into account the effect of valves, pumps and form loss coefficients describing different obstacles in the flow channel.

In order to calculate the flow system numerically Equations (1) to (4) must be discretized in respect to time and space and the non-linear terms must be linearized. The calculation of wall friction F_w, interfacial friction F_i, interfacial heat transfer q_i and wall heat transfer q_w from empirical correlations has a strong effect on the solution. The linearization of these terms depends on the form of each correlation.

The total energy equation was obtained by adding a kinetic energy equation to a one-dimensional form of thermal energy equation.

The following relationships connect the liquid and gas equations:

$$\begin{aligned} \alpha_g &= 1 - \alpha_l = \alpha \\ \Gamma_g &= -\Gamma_l = \Gamma \\ F_{i,l} &= -F_{i,g} = F_i \\ u_{i,g} &= u_{i,l} = u_i \end{aligned} \tag{5}$$

3. Discretization of the governing equations

The discretization and solution principles of the basic six equations follows closely the principles presented in reference /1/. The equations are discretized with respect to space and time and the non-linear terms are linearized. In the space discretization, the staggered discretization scheme has been applied. The mass and energy equations are calculated in the same control volumes, while the control volume of the momentum equation is located between two mass control volumes. The state variables (such as pressure, enthalpy and density of both phases) are calculated in the middle of the mass and energy mesh cells and the flow related variables (such as gas and liquid velocities) are calculated in the momentum mesh cells. In the enthalpy solution, the first order upwind scheme has been utilized. In the mesh cell, the quantities are averaged over the whole mesh. Only in the case of stratified flow the liquid head is taken separately into account in the pressure solution. In the following sections the mass/energy control volumes are called nodes. The momentum control volumes are called branches.

3.1 Discretization of the mass equation

When Equation (1) is multiplied with the cross section of flow A and is integrated over the mesh length Δz, the following equation is obtained:

$$V_i \frac{\partial(\alpha_k \rho_k)}{\partial t} + \Delta(A \alpha_k \rho_k u_k) = V_i \Gamma_k \tag{6}$$

where V_i is the volume of node i ($V_i = A_i \Delta z_i$).

The first term as discretized in respect to time is

$$V_i \frac{\left[(\alpha_k \rho_k)_i^n - (\alpha_k \rho_k)_i^{t-\Delta t}\right]}{\Delta t}. \tag{7}$$

When $(\alpha_k \rho_k)^n$ is linearized in respect to pressure and void fraction, the term (6) is obtained in form

$$V_i \frac{\left[(\alpha_k \rho_k) - (\alpha_k \rho_k)_i^{t-\Delta t}\right]}{\Delta t} + V_i \frac{\alpha_{k,i}}{\Delta t} \frac{\partial \rho_{k,i}}{\partial p_i}\left(p_i^n - p_i\right) + V_i \frac{\rho_{k,i}}{\Delta t}\left(\alpha_{k,i}^n - \alpha_{k,i}\right). \tag{8}$$

In formulas (7) and (8) the superscript n refers to the new iteration step. The variables without superscript are from the previous iteration step and the superscript $t\text{-}\Delta t$ refers to the previous time step.

The second term describes the change of the mass flow of phase *k* over the node. It is discretized over the node *i* from branch *i*-½ to branch *i*+½. First it is obtained

$$\Delta\left(A\alpha_k\rho_k u_k\right)_i^n = A_{i+1/2}\left(\alpha_k\rho_k\right)_{i+1/2}^n u_{k,i+1/2}^n - A_{i-1/2}\left(\alpha_k\rho_k\right)_{i-1/2}^n u_{k,i-1/2}^n \tag{9}$$

where $(\alpha_k\rho_k)_{i+½}$ and $(\alpha_k\rho_k)_{i-½}$ are upwind values. When upwind values are used in the discretization, it is assumed that at the border of two nodes the void fractions, densities and enthalpies are the same as in the nearest node in the direction of coming flow. The new values (superscript *n*) are approximated as follows:

– If the flow is into the node *i* the previous iteration step value $\alpha_k\rho_k$ of the upwind node is used, i.e. the subscript *n* in the term $\left(\alpha_k\rho_k\right)_{i-1/2}$ is omitted.

– If the flow is out of the node i the new value is approximated as

$$\left(\alpha_k\rho_k\right)_{i+1/2}^n = \left(\alpha_k\rho_k\right)_{i+1/2} + \rho_{k,i}\left(\alpha_{k,i}^n - \alpha_{k,i}\right) + \alpha_{k,i}\frac{\partial\rho_{k,i}}{\partial p_i}\left(p_i^n - p_i\right). \tag{10}$$

Finally by combining Equations (9) and (10) for convection term Equation (11) is obtained:

$$\begin{aligned}\Delta\left(A\alpha_k\rho_k u_k\right)_i^n &= A_{i+1/2}\left(\alpha_k\rho_k\right)_{i+1/2} u_{k,i+1/2}^n - A_{i-1/2}\left(\alpha_k\rho_k\right)_{i-1/2} u_{k,i-1/2}^n \\ &+ \left(A_{i+1/2}\left[u_{k,i+1/2},0\right] + A_{i-1/2}\left[-u_{k,i-1/2},0\right]\right)\alpha_{k,i}\frac{\partial\rho_{k,i}}{\partial\rho_i}\left(p_i^n - p_i\right) \\ &+ \left(A_{i+1/2}\left[u_{k,i+1/2},0\right] + A_{i-1/2}\left[-u_{k,i-1/2},0\right]\right)\rho_{k,i}\left(\alpha_{k,i}^n - \alpha_{k,i}\right)\end{aligned} \tag{11}$$

The right hand side term of Equation (6) is linearized as follows:

$$V_i\Gamma_{k,i}^n = V_i\Gamma_{k,i} + V_i\frac{\partial\Gamma_{k,i}}{\partial\alpha_{k,i}}\left(\alpha_{k,i}^n - \alpha_{k,i}\right). \tag{12}$$

The linearization is used when the mass equation is applied in the void fraction solution.

By taking into account the formulas (8), (11) and (12) the linearized mass equation can be presented as

$$
\begin{aligned}
& V_i \frac{\left[\left(\alpha_k \rho_k\right)_i - \left(\alpha_k \rho_k\right)_i^{t-\Delta t}\right]}{\Delta t} + V_i \frac{\alpha_{k,i}}{\Delta t} \frac{\partial \rho_{k,i}}{\partial p_i} \left(p_i^n - p_i\right) \\
& + V_i \frac{\rho_{k,i}}{\Delta t} \left(\alpha_{k,i}^n - \alpha_{k,i}\right) + A_{i+1/2} \left(\alpha_k \rho_k\right)_{i+1/2} u_{k,i+1/2}^n - A_{i-1/2} \left(\alpha_k \rho_k\right)_{i-1/2} u_{k,i-1/2}^n \\
& + A_{i+1/2} \left[u_{k,i+1/2}, 0\right] \alpha_{k,i} \frac{\partial \rho_{k,i}}{\partial p_i} \left(p_i^n - p_i\right) + A_{i+1/2} \left[u_{k,i+1/2}, 0\right] \rho_{k,i} \left(\alpha_{k,i}^n - \alpha_{k,i}\right) \\
& + A_{i-1/2} \left[-u_{k,i-1/2}, 0\right] \alpha_{k,i} \frac{\partial \rho_{k,i}}{\partial p_i} \left(p_i^n - p_i\right) + A_{i-1/2} \left[-u_{k,i-1/2}, 0\right] \rho_{k,i} \left(\alpha_{k,i}^n - \alpha_{k,i}\right) \\
& = V_i \Gamma_{k,i} + V_i \frac{\partial \Gamma_{k,i}}{\partial \alpha_{k,i}} \left(\alpha_{k,i}^n - \alpha_{k,i}\right)
\end{aligned}
\tag{13}
$$

3.2 Discretization of the momentum equation

When Equation (2) is multiplied with the average cross section of branch i+½ ($A_{i+½}$) and integrated over the length of branch i+½ ($\Delta z_{i+½}$), the following equation is obtained:

$$
V_{i+1/2} \frac{\partial \left(\alpha_k \rho_k u_k\right)_{i+1/2}}{\partial t} + \Delta \left(A \alpha_k \rho_k u_k^2\right)_{i+1/2} A_{i+1/2} \rho_{k,i+1/2} \Delta p_{i+1/2} = S_{i+1/2} . \tag{14}
$$

In Equation (14) the term S is the right hand side of Equation (2).

The discretization of the first term of the momentum equation is straight-forward and hence it is obtained:

$$
V_{i+1/2} \frac{\left(\overline{\alpha_k \rho_k}\right)_{i+1/2} u_{k,i+1/2}^n - \left(\overline{\alpha_k \rho_k}\right)_{i+1/2}^{t-\Delta t} u_{k,i+1/2}^{t-\Delta t}}{\Delta t} . \tag{15}
$$

Here the volume $V_{i+½}$ is the volume of the branch i+½ ($V_{i+½} = A_{i+½} \Delta z_{i+½}$).

In the discretization of the momentum flow term the upwind discretization is applied. Hence, the second term as discretized is calculated:

$$
\begin{aligned}
& A_{i+1/2} \left(\alpha_k \rho_k\right)_{i+1/2} u_{k,i+1/2}^2 + 2 A_{i+1/2} \left(\alpha_k \rho_k\right)_{i+1/2} u_{k,i+1/2} \left(u_{k,i+1/2}^n - u_{k,i+1/2}\right) \\
& - A_{i-1/2} \left(\alpha_k \rho_k\right)_{i-1/2} u_{k,i+1/2}^2 \quad ; \quad if \quad u_{k,i+1/2} \geq 0
\end{aligned}
\tag{16}
$$

or

$$A_{i+3/2}\left(\alpha_k\rho_k\right)_{i+3/2}\,u^2_{k,i+3/2} - 2A_{i+1/2}\left(\alpha_k\rho_k\right)_{i+1/2}u_{k,i+1/2}\,\left(u^n_{k,i+1/2}-u_{k,i+1/2}\right)$$
$$- A_{i+1/2}\left(\alpha_k\rho_k\right)_{i+1/2}u^2_{k,i+1/2} \quad ; \quad if \quad u_{k,i+1/2}<0 \tag{17}$$

In Equations (16) and (17) the linearization has been done only in respect to $u_{k,i+½}$. This enables the direct solution of the velocities and no matrix solution of velocities is needed.

In Equations (16) and (17) the new value of $u_{k,i+½}$ is approximated as

$$\left(u^n_{k,i+1/2}\right)^2 = u^2_{k,i+1/2} + 2u_{k,i+1/2}\,\left(u^n_{k,i+1/2}-u_{k,i+1/2}\right). \tag{18}$$

The third term of the momentum equation is simply

$$A_{i+1/2}\,\overline{\alpha}_{k,i+1/2}\,\left(p^n_{i+1}-p^n_i\right). \tag{19}$$

The fourth term as discretized can be expressed as

$$V_{i+1/2}\,\overline{\Gamma}_{k,i+1/2}\,u^n_{i,\,i+1/2}\,. \tag{20}$$

In Equation (20) the interface velocity is calculated as follows:

$$u^n_{i,i+1/2} = \beta u^n_{g,i+1/2} + \left(1-\beta\right)u^n_{l,i+1/2}\,. \tag{21}$$

For β the value 0.5 is commonly used, but also $\beta = \alpha_g$ has been applied.

The fifth term as discretized is

$$V_{i+1/2}\left(\overline{\alpha_k\,\rho_k}\right)_{i+1/2}\,\vec{g}\,. \tag{22}$$

The sixth, the wall friction term as discretized is

$$V_{i+1/2}\,F^n_{wk} = V_{i+1/2}\,F_{wk} + V_{i+1/2}\,\frac{\partial F_{wk}}{\partial u_k}\,\left(u^n_{k,i+1/2}+u_{k,i+1/2}\right). \tag{23}$$

The seventh, interfacial friction term is discretized as follows:

$$V_{i+1/2}\,F^n_{ik} = V_{i+1/2}\,F_{ik} + V_{i+1/2}\,\frac{\partial F_{ik}}{\partial \Delta u}\,\left(\Delta u^n_{i+1/2}-\Delta u_{\,i+1/2}\right) \tag{24}$$

where $\Delta u_{i+1/2}$ is the difference between phase velocities, i.e. $\Delta u_{i+1/2} = u_{g,i+1/2} - u_{l,i+1/2}$.

The friction loss of valves is as discretized

$$-1/2\, A_{i+1/2}\, C_{v,\,i+1/2} \left(\overline{\alpha_k \rho_k}\right)_{i+1/2} u^n_{k,\,i+1/2} \left|u^n_{k,\,i+1/2}\right| = f_1\left(u^n_{k,\,i+1/2}\right). \tag{25}$$

Assuming that the friction coefficient C_v of a valve is not dependent on velocity, the linearized friction loss term can be expressed as

$$\begin{aligned} & f_1\left(u_{k,i+1/2}\right) + \frac{\partial f_1\left(u_{k,i+1/2}\right)}{\partial u_k}\left(u^n_{k,i+1/2} - u_{k,i+1/2}\right) \\ & = -1/2\, A_{i+1/2}\, C_{v,i+1/2} \left(\overline{\alpha_k \rho_k}\right)_{i+1/2} \left|u_{k,i+1/2}\right| \left(2u^n_{k,i+1/2} - u_{k,i+1/2}\right) \end{aligned} \tag{26}$$

The friction loss resulting from form loss coefficients C_{fl} is linearized in the same manner. The pump head term is discretized and linearized as follows:

$$\begin{aligned} & A_{i+1/2}\, \bar{\alpha}_{k,i+1/2}\; 1/2 \Delta p^n_{pu,i+1/2} \\ & = A_{i+1/2}\, \bar{\alpha}_{k,i+1/2} \left[\Delta p_{pu,i+1/2} + \frac{\partial \Delta p_{pu,\,i+1/2}}{\partial u_k}\left(u^n_{k,\,i+1/2} - u_{k,i+1/2}\right)\right] \end{aligned} \tag{27}$$

Finally the discretized momentum equation is obtained:

$$\begin{aligned} & V_{i+1/2}\, \frac{\left(\overline{\alpha_k\, \rho_k}\right)_{i+1/2}\, u^n_{k,i+1/2} - \left(\overline{\alpha_k\, \rho_k}\right)^{t-\Delta t}_{i+1/2}\, u^{t-\Delta t}_{k,i+1/2}}{\Delta t} \\ & \quad + \Delta\left(A \alpha_k\, \rho_k\, u_k^2\right)^n_{i+1/2} + A_{i+1/2}\, \bar{\alpha}_{k,i+1/2}\left(p^n_{i+1} - p^n_i\right) \\ & = V_{i+1/2}\, \overline{\Gamma}_{k,i+1/2}\, u^n_{i,\,i+1/2} + V_{i+1/2}\left(\overline{\alpha_k \rho_k}\right)_{i+1/2} \vec{g} \\ & \quad + V_{i+1/2}\, F_{wk,i+1/2} + V_{i+1/2}\, \frac{\partial F_{wk,i+1/2}}{\partial u_k}\left(u^n_{k,i+1/2} - u_{k,i+1/2}\right) \\ & \quad + V_{i+1/2}\, F_{ik,i+1/2} + V_{i+1/2}\, \frac{\partial F_{ik,i+1/2}}{\partial \Delta u}\left(\Delta u^n_{i+1/2} - \Delta u_{\,i+1/2}\right) \\ & \quad - 1/2\, A_{i+1/2}\left(C_v + C_{f1}\right)_{i+1/2} \left(\overline{\alpha_k\, \rho_k}\right)_{i+1/2} \left|u_{k,i+1/2}\right| \left(2u^n_{k,i+1/2} - u_{k,i+1/2}\right) \\ & \quad + A_{i+1/2}\, \bar{\alpha}_{k,i+1/2}\left[\Delta p_{pu,i+1/2} + \frac{\partial \Delta p_{pu,i+1/2}}{\partial u_k}\left(u^n_{k,i+1/2} - u_{k,i+1/2}\right)\right] \end{aligned} \tag{28}$$

The term $\Delta(A\,\alpha_k \rho_k u_k^2)^n_{i+1/2}$ is calculated as shown in Equations (16) and (17).

3.3 Discretization of the energy equation

By multiplying Equation (3) with the average cross section of node *i* and by integrating over the node *i* the following equation (29) is obtained ($V_i = A_i \Delta z_i$):

$$V_i \frac{\partial(\alpha_k \rho_k h_k)_i}{\partial t} + \Delta(A \alpha_k \rho_k u_k h_k)_i = V_i \alpha_{k,i} \frac{\partial p_i}{\partial t} + V_i \Gamma_{k,i} h_{ik,i} + V_i q_{ik,i} + V_i q_{wk,i} + V_i F_{ik,i} u_{i,i} + V_i (\alpha_k \rho_k u_k \vec{g})_i \tag{29}$$

The first term of Equation (29) as discretized is

$$V_i \frac{\alpha_{k,i} \rho_{k,i} h_{k,i}^n - (\alpha_{k,i} \rho_{k,i} h_{k,i})^{t-\Delta t}}{\Delta t}. \tag{30}$$

Using upwind discretization, the second term (convection) becomes

$$\begin{aligned} & A_{i+1/2} (\alpha_k \rho_k)_{i+1/2} [u_{k,i+1/2}, 0] h_{k,i}^n \\ & - A_{i-1/2} (\alpha_k \rho_k)_{i-1/2} [u_{k,i-1/2}, 0] h_{k,i-1}^n \\ & + A_{i-1/2} (\alpha_k \rho_k)_{i-1/2} [-u_{k,i-1/2}, 0] h_{k,i}^n \\ & - A_{i+1/2} (\alpha_k \rho_k)_{i+1/2} [-u_{k,i+1/2}, 0] h_{k,i+1}^n \end{aligned} \tag{31}$$

The discretization of the first (pressure change), second (mass transfer) and fourth terms (wall heat transfer) on the right hand side is straight-forward. The phase enthalpies at the interface used in the mass transfer term are calculated assuming saturated conditions:

$$h_{ik} = h_{k,sat} + u_k u_i - \frac{u_k^2}{2}. \tag{32}$$

For the third term of the right hand side, the heat transfer between interface and gas and liquid phases is calculated

$$q_{ik} = -K_{ik,i} (h_{k,stat}^n - h_{k,sat}) \tag{33}$$

and as discretized the third term can be written

$$-V_i K_{ik,i} (h_{k,stat}^n - h_{k,sat}) + V_i K_{ik,i} \frac{(u_{k,i+1/2} + u_{k,i-1/2})^2}{8} \tag{34}$$

where the static enthalpy $h^n_{k,stat} = h^n_{k,i} - u^2_{k,i}/2$ and the node velocity $u_{k,i} = (u_{k,i+1/2} + u_{k,i-1/2})/2$.

In the rest of the terms the node velocities are calculated as an average of the connecting branch velocities and the interface velocity is calculated as an average of phase node velocities. These terms for interface friction and potential energy terms are not currently used in the two-phase flow model of APROS.

Finally the discretized energy equation can be expressed in the form

$$\begin{aligned}
&\left\{ A_{i+1/2}\left(\alpha_k \rho_k\right)_{i+1/2}\left[u_{k,i+1/2},0\right] + A_{i-1/2}\left(\alpha_k \rho_k\right)_{i-1/2}\left[-u_{k,i-1/2},0\right] + V_i\left[K_{ik,i}\frac{h_s}{kg} + \frac{\left(\alpha_k \rho_k\right)_i}{\Delta t}\right]\right\} h^n_{k,i} \\
&- A_{i+1/2}\left(\alpha_k \rho_k\right)_{i+1/2}\left[-u_{k,i+1/2},0\right] h^n_{k,i+1} \\
&- A_{i-1/2}\left(\alpha_k \rho_k\right)_{i-1/2}\left[-u_{k,i-1/2},0\right] h^n_{k,i-1} \\
&= V_i \left[\begin{array}{l} \alpha_{k,i}\dfrac{p_i - p_i^{t-\Delta t}}{\Delta t} + \Gamma_k h_{ik,i} + F_{ik,i} u_{i,i} + \left(\alpha_k \rho_k\right)_i u_{k,i}\vec{g} + \dfrac{\left(\alpha_k \rho_k\right)_i^{t-\Delta t} h_{k,i}^{t-\Delta t}}{\Delta t} \\ + K_{ik,i} h_{k\,sat,i} + \dfrac{K_{ik,i}}{8}\left(u_{k,i+1/2} + u_{k,i-1/2}\right)^2 + q_{wk,i} \end{array} \right]
\end{aligned} \tag{35}$$

3.4 Discretization of the non-condensable gas mass equation

For the numerical solution of the non-condensable gas density the partial differential equation (4) has to be descretized in respect of time and space.

For the time discretization the time derivative is simply taken in form

$$V_i \frac{\left(\alpha_g \rho^n_{nc}\right)_i - \left(\alpha_g \rho_{nc}\right)_i^{t-\Delta t}}{\Delta t}. \tag{36}$$

In Equation (36) the subscript i refers to the mass control volume and the subscript nc refers to non-condensable gas. The superscript n is new iteration step and t-Δt means the previous time step.

For the space discretization Equation (4) is multiplied with the cross section of flow path A and it is integrated over the node length Δz. Then using the upwind approach to the convective term the partial differential equation (4) as descretized Equation (37) is obtained

$$V_i \frac{\alpha_{g,i}}{\Delta t}\rho^n_{nc,i} - V_i \frac{\left(\alpha_g \rho_{nc}\right)_i^{t-\Delta t}}{\Delta t} + A_{i+1/2}\alpha_{g,i+1/2}\left[u_{g,i+1/2},0\right]\rho^n_{nc,i}$$
$$- A_{i-1/2}\alpha_{g,i-1/2}\left[u_{g,i-1/2},0\right]\rho^n_{nc,i-1} + A_{i-1/2}\alpha_{g,i-1/2}\left[-u_{g,i-1/2},0\right]\rho^n_{nc,i} \qquad (37)$$
$$- A_{i+1/2}\alpha_{g,i+1/2}\left[-u_{g,i+1/2},0\right]\rho^n_{nc,i+1} = 0$$

In equation the non-condensable gas densities with superscript n are unknowns. By rearranging terms in Equation (37) the matrix type equation (38) is obtained:

$$a_i \rho^n_{nc,i} = a_{i+1}\rho^n_{nc,i+1} + a_{i-1}\rho^n_{nc,i-1} + b_i \,. \qquad (38)$$

In Equation (38) the following abbreviations have been used:

$$a_i = V_i \frac{\alpha_{g,i}}{\Delta t} + A_{i+1/2}\alpha_{g,i+1/2}\left[u_{g,i+1/2},0\right] + A_{i-1/2}\alpha_{g,i-1/2}\left[-u_{g,i-1/2},0\right] \qquad (39)$$

$$a_{i+1/2} = A_{i+1/2}\alpha_{g,i+1/2}\left[-u_{g,i+1/2},0\right] \qquad (40)$$

$$a_{i-1} = A_{i-1/2}\alpha_{g,i-1/2}\left[u_{g,i-1/2},0\right] \qquad (41)$$

$$b_i = V_i \frac{\left(\alpha_g \rho_{nc}\right)_i^{t-\Delta t}}{\Delta t} \,. \qquad (42)$$

In Equations (39) to (41) the branch void fractions are used as upwind values, i.e. using the value of the node where flow comes from.

4. Solution procedure

The final equations for each variable to be solved are obtained from the discretized equations derived in Chapter 3. The pressure equation is formed from the mass and momentum equations by eliminating the velocities and void fractions. After the pressures are solved the velocities can be calculated directly using the coefficients of the pressure equation and the new pressures. The void fraction solution is obtained from the mass equations of liquid and gas and the enthalpy solution from the energy equations. The non-condensable gas densities are solved from discretized non-condensable gas mass equation.

The solution of the two-phase flow system is obtained via an iterative procedure. Before the iteration, the material properties of each phase (density, saturation enthalpy, temperature, heat capacity, viscosity and heat conductivity) are calculated as functions of pressure and enthalpy. The solution procedure has the following steps:

1. The state of the pumps and valves in iteration is computed.
2. Interfacial heat transfer coefficients are calculated.
3. The pressure equation is formed and pressures are solved.
4. The velocities are calculated.
5. The densities, saturation enthalpies and temperatures are updated using the new pressures.
6. The void fraction equation is formed and void fractions are solved.
7. The non-condensable gas equation is formed and the non-condensable densities are solved.
8. The heat flows from heat structures are calculated and the temperatures of the heat structures connected to the flow model are solved.
9. The enthalpies are solved.
10. Interfacial mass transfer rates are calculated using the interfacial heat transfer coefficients and the new enthalpies.
11. The convergence of the iteration is checked by comparing the mass errors to the maximum allowed values. If the mass error in some node is too large, the iteration cycle is repeated.
12. If the iteration has converged, boron concentrations are solved using the new state of the flow system.

The derivation of each linear equation group to be solved is discussed in the following sections.

4.1 Solution of flows and pressures

When the discretized momentum equation (28) is applied for gas phase (k = g) and liquid phase (k = l) the following equations are obtained:

$$\begin{aligned} a_g u^n_{g,i+1/2} &= b_g\left(p^n_{i+1} - p^n_i\right) + c_g u^n_{1,i+1/2} + d_g \\ a_1 u^n_{1,i+1/2} &= b_1\left(p^n_{i+1} - p^n_i\right) + c_1 u^n_{g,i+1/2} + d_1 \end{aligned} \tag{43}$$

From Equations (43) both of the phase velocities can be solved:

$$u^n_{k,i+1/2} = D_{k,i+1/2}\left(p^n_{i+1} - p^n_i\right) + U_{k,i+1/2}\,. \tag{44}$$

In Equation (44) the terms for gas phase are

$$D_{g,i+1/2} = \frac{b_g + c_g\, b_1/a_1}{a_g - c_1\, c_g/a_1}\,, \quad U_{g,i+1/2} = \frac{d_g + c_g\, d_1/a_1}{a_g - c_1\, c_g/a_1} \tag{45}$$

and the terms for liquid phase are

$$D_{1,i+1/2} = \frac{b_1 + c_1\, b_g/a_g}{a_1 - c_1\, c_g/a_g}\,, \quad U_{1,i+1/2} = \frac{d_1 + c_1\, d_g/a_g}{a_1 - c_1\, c_g/a_g}\,. \tag{46}$$

The coefficients in Equations (43) are as follows, first for the gas phase:

$$\begin{aligned} a_g = {} & \frac{V_{i+1/2}\left(\overline{\alpha\rho_g}\right)_{i+1/2}}{\Delta t} + 2A_{i+1/2}\left(\alpha\rho_g\right)_{i+1/2}\left|u_{g,\,i+1/2}\right| \\ & + V_{i+1/2}\left(-\beta\overline{\Gamma}_{i+1/2} - \frac{\partial F_{wg,i+1/2}}{\partial u_g} + \frac{\partial F_{i,i+1/2}}{\partial \Delta u}\right) \\ & + 2A_{i+1/2}\left(C_v + C_{f1}\right)_{i+1/2}\left(\overline{\alpha\rho_g}\right)_{i+1/2}\left|u_{g,\,i+1/2}\right| \\ & - A_{i+1/2}\,\overline{\alpha}_{i+1/2}\,\frac{\partial \Delta p_{pu,\,i+1/2}}{\partial u_g} \end{aligned} \tag{47}$$

$$b_g = -A_{i+1/2}\,\overline{\alpha}_{i+1/2} \tag{48}$$

$$c_g = V_{i+1/2}\left[\frac{\partial F_{i,i+1/2}}{\partial \Delta u} + (1-\beta)\,\overline{\Gamma}_{i+1/2}\right] \tag{49}$$

$$\begin{aligned} d_g = {} & V_{i+1/2}\left[\left(\overline{\alpha\rho_g}\right)_{i+1/2}\vec{g} + F_{wg,i+1/2} - \frac{\partial F_{wg,i+1/2}}{\partial u_g}u_{g,i+1/2} - F_{i,i+1/2} + \frac{\partial F_{i,i+1/2}}{\partial \Delta u}\left(u_{g,i+1/2} - u_{1,i+1/2}\right)\right] \\ & + \frac{V_{i+1/2}\left(\overline{\alpha\rho_g}\right)^{t-\Delta t}_{i+1/2}\,u^{t-\Delta t}_{g,i+1/2}}{\Delta t} + M_{g,FL} \\ & + A_{i+1/2}\left(C_v + C_{f1}\right)_{i+1/2}\left(\overline{\alpha\rho_g}\right)_{i+1/2}u_{g,i+1/2}\left|u_{g,i+1/2}\right| \\ & + A_{i+1/2}\,\overline{\alpha_{i+1/2}}\left(\Delta p_{pu,i+1/2} - \frac{\Delta p_{pu,i+1/2}}{\partial u_g}\,u_{g,i+1/2}\right) \end{aligned} \tag{50}$$

The quantity $M_{g,FL}$ is a part of the gas momentum flow term and it is calculated as

$$\begin{aligned} & M_{g,FL} = A_{i+1/2}\left(\alpha\rho_g\right)_{i+1/2}u^2_{g,i+1/2} + A_{i-1/2}\left(\alpha\rho_g\right)_{i-1/2}u^2_{g,i-1/2} \\ & ;\quad if\quad u_{g,i+1/2} > 0 \end{aligned} \tag{51}$$

or

$$\begin{aligned} & M_{g,FL} = -A_{i+3/2}\left(\alpha\rho_g\right)_{i+3/2}u^2_{g,i+3/2} - A_{i+1/2}\left(\alpha\rho_g\right)_{i+1/2}u^2_{g,i+1/2} \\ & ;\quad if\quad u_{g,i+1/2} < 0 \end{aligned} \tag{52}$$

The corresponding coefficients for the liquid phase are

$$\begin{aligned} a_1 = {} & \frac{V_{i+1/2}\left[\overline{(1-\alpha)\rho_1}\right]_{i+1/2}}{\Delta t} + 2A_{i+1/2}\left[(1-\alpha)\rho_1\right]_{i+1/2}\left|u_{1,i+1/2}\right| \\ & + V_{i+1/2}\left[(1-\beta)\overline{\Gamma}_{i+1/2} - \frac{\partial F_{w1,i+1/2}}{\partial u_1} + \frac{\partial F_{i,i+1/2}}{\partial \Delta u}\right] \\ & + 2A_{i+1/2}\left(C_v + C_{f1}\right)_{i+1/2}\left[\overline{(1-\alpha)\rho_1}\right]_{i+1/2}\left|u_{1,i+1/2}\right| \\ & - A_{i+1/2}\left(1-\overline{\alpha}_{i+1/2}\right)\frac{\partial \Delta p_{pu,i+1/2}}{\partial u_1} \end{aligned} \tag{53}$$

$$b_1 = -A_{i+1/2}\left(1-\overline{\alpha}_{i+1/2}\right) \tag{54}$$

$$c_1 = V_{i+1/2}\left(\frac{\partial F_{i,i+1/2}}{\partial \Delta u} - \beta\overline{\Gamma}_{i+1/2}\right) \tag{55}$$

$$
\begin{aligned}
d_1 = V_{i+1/2} \Bigg\{ & \left[\overline{(1-\alpha)\rho_1}\right]_{i+1/2} \vec{g} + F_{w1,i+1/2} - \frac{\partial F_{w1,i+1/2}}{\partial u_1} u_{1,i+1/2} + F_{i,i+1/2} - \frac{\partial F_{i,i+1/2}}{\partial \Delta u} \left(u_{g,i+1/2} - u_{1,i+1/2} \right) \Bigg\} \\
& + \frac{V_{i+1/2} \left[\overline{(1-\alpha)\rho_1}\right]_{i+1/2}^{t-\Delta t} \; u_{i+1/2}^{t-\Delta t}}{\Delta t} + M_{1,FL} \\
& + A_{i+1/2} \left(C_v + C_{f1} \right)_{i+1/2} \left[\overline{(1-\alpha)\rho_1}\right]_{i+1/2} u_{1,i+1/2} \left| u_{1,i+1/2} \right| \\
& + A_{i+1/2} \left(1 - \overline{\alpha}_{i+1/2} \right) \left(\Delta p_{pu,i+1/2} - \frac{\partial \Delta p_{pu,i+1/2}}{\partial u_1} u_{1,i+1/2} \right)
\end{aligned}
\tag{56}
$$

The variable $M_{l,FL}$ is calculated analogously to the gas phase variable $M_{g,FL}$.

The next step in developing the pressure solution is to replace the velocities $u^n_{g,i+1/2}$, $u^n_{g,i-1/2}$, $u^n_{1,i+1/2}$ and $u^n_{1,i-1/2}$ in both mass equations (Equation 13 for liquid and gas) with formula (44). From the two equations obtained in this way the term $\alpha^n_{k,i} - \alpha_{k,i}$ is eliminated and the following equation results:

$$
a_i p^n_i = a_i p^n_{i+1} + a_{i-1} p^n_{i-1} + b_i \,. \tag{57}
$$

In Equation (57) the coefficients are as follows:

$$
a_{i+1} = -A_{i+1/2} \left\{ \frac{\left[(1-\alpha)\rho_1\right]_{i-1/2} D_{1,i+1/2}}{f_{1,i}} + \frac{\left(\alpha\rho_g\right)_{i+1/2} D_{g,i+1/2}}{f_{g,i}} \right\} \tag{58}
$$

$$
a_{i\text{-}1} = -A_{i\text{-}1/2} \left\{ \frac{\left[(1-\alpha)\rho_1\right]_{i-1/2} D_{1,i\text{-}1/2}}{f_{1,i}} + \frac{\left(\alpha\rho_g\right)_{i\text{-}1/2} D_{g,i\text{-}1/2}}{f_{g,i}} \right\} \tag{59}
$$

$$
a_i = a_{i+1} + a_{i-1} + \frac{e_{1,i}}{f_{1,i}} + \frac{e_{g,i}}{f_{g,i}} \tag{60}
$$

$$
b_i = -\frac{\Delta m_{g,i}}{f_{g,i}} - \frac{\Delta m_{1,i}}{f_{1,i}} + \left(\frac{e_{1,i}}{f_{1,i}} + \frac{e_{g,i}}{f_{g,i}} \right) p_i \,. \tag{61}
$$

In Equations (59) to (61) the following notations have been used:

$$
f_{k,i} = \rho_{k,i} \left(\frac{V_i}{\Delta t} + A_{i+1/2} \left[u_{k,i+1/2}, 0 \right] + A_{i-1/2} \left[-u_{k,i-1/2}, 0 \right] \right) \tag{62}
$$

$$e_{k,i} = \alpha_{k,i} \frac{\partial \rho_{k,i}}{\partial p_i} \left(\frac{V_i}{\Delta t} + A_{i+1/2} \left[u_{k,i+1/2}, 0 \right] + A_{i-1/2} \left[-u_{k,i-1/2}, 0 \right] \right) + \frac{\left| \Delta m_{k,i} \right|}{\Delta p_{\max i}} \tag{63}$$

$$\begin{aligned} \Delta m_{k,i} = V_i \frac{\left(\alpha_k \rho_k \right)_i - \left(\alpha_k \rho_k \right)_i^{t-\Delta t}}{\Delta t} + A_{i+1/2} \left(\alpha_k \rho_k \right)_{i+1/2} U_{k,i+1/2} \\ - A_{i-1/2} \left(\alpha_k \rho_k \right)_{i-1/2} U_{k,i-1/2} - V_i \Gamma_{k,i} \end{aligned} \tag{64}$$

In Equations (62) to (64) the subscript *k* refers either to *l* (liquid) or to *g* (gas). The last term of coefficient e_k is a relaxation term that limits the change of the pressure between two iterations. The variable Δp_{max} means the maximum allowed change of pressure between two succeeding iterations.

Even if Equation (57) has been deduced assuming that the node *i* is connected to two other nodes *i*-1 and *i*+1, the equation can be applied for a general case where the node i is connected to an arbitrary number of nodes. In that case all terms for branch *i*+1/2 are replaced by a sum of similar terms for all branches leaving from the node. The index *i*-1/2 denotes the branches coming to node *i*. In Equations (16) and (17) the momentum flow terms with index *i*-1/2 and *i*+3/2 are replaced by the sum of the momentum flows of all branches flowing into the upwind node. The incoming momentum flow is then distributed between all branches where the flow is out of the node. The ratios of the branch flow areas and the sum of the areas of all outgoing branches determine the distribution. It is also possible to define the branches which do not transmit momentum. For these branches the term $\Delta \alpha_k \rho_k u_k^2$ is set to zero and they do not contribute to the corresponding term of other branches.

When the equations for all nodes *i* which belong to the simulated system have been written, a linear equation group for pressures is obtained and the pressures can be solved simultaneously.

After the pressures p^n_i have been solved the phase velocities u_g and u_l for all branches can be calculated directly by using Equation (44).

4.2 Solution of void fractions

The void fraction solution is based on the mass equations of the liquid and gas phases (13). From Equation (13) for gas the following equation is obtained:

$$a_i \alpha_i^n = a_{i+1} \alpha_{i+1}^n + a_{i-1} \alpha_{i-1}^n + b_i \tag{65}$$

where

$$a_i = \frac{V_i \rho_{g,i}}{\Delta t} + A_{i+1/2}\rho_{g,i}\left[u_{g,i+1/2},0\right] + A_{i-1/2}\rho_{g,i}\left[-u_{g,i-1/2},0\right] - V_i\frac{\partial \Gamma_i}{\partial \alpha_i} \tag{66}$$

$$a_{i+1} = A_{i+1/2}\rho_{g,i+1}\left[-u_{g,i+1/2},0\right] \tag{67}$$

$$a_{i\text{-}1} = A_{i\text{-}1/2}\rho_{g,i\text{-}1}\left[u_{g,i-1/2},0\right] \tag{68}$$

$$b_i = \frac{V_i\left(\alpha\rho_g\right)_i^{t-\Delta t}}{\Delta t} + V_i\Gamma_i - V_i\frac{\partial \Gamma_i}{\partial \alpha_i}\alpha_i . \tag{69}$$

Analogously for liquid the following equation is obtained:

$$\mathrm{a_i}\left(1-\alpha_\mathrm{i}^\mathrm{n}\right) = \mathrm{a_{i+1}}\left(1-\alpha_{\mathrm{i+1}}^\mathrm{n}\right) + \mathrm{a_{i-1}}\left(1-\alpha_{\mathrm{i-1}}^\mathrm{n}\right) + \mathrm{b_i} . \tag{70}$$

In Equation (70) the coefficients are as follows:

$$a_i = \frac{V_i \rho_{1,i}}{\Delta t} + A_{i+1/2}\rho_{1,i}\left[u_{l,i+1/2},0\right] + A_{i-1/2}\rho_{1,i}\left[u_{l,i+1/2},0\right] - V_i\frac{\partial \Gamma_i}{\partial \alpha_i} \tag{71}$$

$$a_{i+1} = A_{i+1/2}\rho_{1,i+1}\left[-u_{l,i+1/2},0\right] \tag{72}$$

$$a_{i\text{-}1} = A_{i\text{-}1/2}\rho_{1,i-1}\left[u_{l,i-1/2}\right] \tag{73}$$

$$b_i = \frac{V_i\left[\left(1-\alpha\right)\rho_1\right]_i^{t-\Delta t}}{\Delta t} - V_i\Gamma_i - V_i\frac{\partial \Gamma_i}{\partial \alpha_i}\left(1-\alpha_i\right). \tag{74}$$

The final void fraction solution system is obtained by summing Equations (65) and (70). However, if the previously calculated void fraction is 0 in some node, only Equation (65) is used in that node. If void fraction is 1, only Equation (70) is used. In single-phase flow this procedure prevents the erroneous formation of the other phase because of the error in mass balances.

When Equations (65) and/or (70) are applied for all the nodes i, a linear equation group is obtained for the simultaneous solution of all void fractions. If both equations are used, the resulting void fraction equation is as follows:

$$a_i \alpha_i^n = a_{i+1} \alpha_{i+1}^n + a_{i-1} \alpha_{i-1}^n + b_i \tag{75}$$

where

$$\begin{aligned} a_i = & \frac{V_i \left(\rho_{g,i} + \rho_{1,i} \right)}{\Delta t} + A_{i+1/2} \rho_{g,i} \left[u_{g,i+1/2}, 0 \right] \\ & + A_{i-1/2} \rho_{g,i} \left[-u_{g,i-1/2}, 0 \right] + A_{i+1/2} \rho_{1,i} \left[u_{1,i+1/2}, 0 \right] \\ & + A_{i-1/2} \rho_{1,i} \left[-u_{1,i-1/2}, 0 \right] - 2 V_i \frac{\partial \Gamma_i}{\partial \alpha_i} \end{aligned} \tag{76}$$

$$a_{i+1} = A_{i+1/2} \rho_{g,i+1} \left[-u_{g,i+1/2}, 0 \right] + A_{i+1/2} \rho_{1,i+1} \left[-u_{1,i+1/2}, 0 \right] \tag{77}$$

$$a_{i\text{-}1} = A_{i\text{-}1/2} \rho_{g,i-1} \left[u_{g,i-1/2}, 0 \right] + A_{i\text{-}1/2} \rho_{1,i-1} \left[u_{1,i\text{-}1/2}, 0 \right] \tag{78}$$

$$\begin{aligned} b_i = & \frac{V_i \left(\alpha \rho_g \right)_i^{t-\Delta t}}{\Delta t} - \frac{V_i \left[(1-\alpha) \rho_1 \right]_i^{t-\Delta t}}{\Delta t} + \frac{V_i \rho_{1,i}}{\Delta t} \\ & + 2 V_i \Gamma_i - 2 V_i \frac{\partial \Gamma_i}{\partial \alpha_i} \alpha_i + A_{i+1/2} \rho_{1,i} \left[u_{1,i+1/2}, 0 \right] \\ & + A_{i-1/2} \rho_{1,i} \left[-u_{1,i-1/2}, 0 \right] - A_{i+1/2} \rho_{1,i+1} \left[-u_{1,i+1/2}, 0 \right] \\ & - A_{i-1/2} \rho_{1,i-1} \left[u_{1,i-1/2}, 0 \right] \end{aligned} \tag{79}$$

If the previous void fraction is 0 in some node, all terms containing the gas density are left out of the coefficients in formulas (76) to (79). If the previous void fraction is 1, all terms containing the liquid density are left out. In both these cases the multiplier 2 in the terms containing mass transfer rate or its derivative is changed to 1.

4.3 Solution of non-condensable gas densities

After the flows the phase flows have been calculated and the gas void fraction have been solved the non-condensable gas densities can be solved. Equations (38) to (42) form the linear equation group, which can directly be solved using a matrix solver.

4.4 Solution of enthalpies

When the void fractions have been solved and the phase velocities have been calculated the enthalpy solution for both phase enthalpies is obtained directly from Equation (35).

For the liquid phase the equation can be written in the form

$$a_{1,i}h^n_{1,i} = a_{1,i+1}h^n_{1,i+1} + a_{1,i-1}h^n_{1,i-1} + b_{1,i}\,. \tag{80}$$

Analogously for the gas phase the following equation is obtained:

$$a_{g,i}h^n_{g,i} = a_{g,i+1}h^n_{g,i+1} + a_{g,i-1}h^n_{g,i-1} + b_{g,i}\,. \tag{81}$$

The coefficients $a_{k,i}$, $a_{k,i+1}$, $a_{k,i-1}$ and $b_{k,i}$ can be calculated by comparing Equations (80), (81) and (35). Hence, it is obtained

$$\begin{aligned} a_{k,i} = {} & A_{i+1/2}\left(\alpha_k\rho_k\right)_{i+1/2}\left\lfloor u_{k,i+1/2},0\right\rfloor + A_{i-1/2}\left(\alpha_k\rho_k\right)_{i-1/2}\left\lfloor -u_{k,i-1/2},0\right\rfloor \\ & + V_i\left[K_{ik,i} + \frac{\left(\alpha_k\rho_k\right)_i}{\Delta t}\right] + \frac{\left|S_{k,i}\right|}{\Delta h_{k\max}} + \left[-\Delta m_{k,i},0\right] \end{aligned} \tag{82}$$

$$a_{k,i+1} = A_{i+1/2}\left(\alpha_k\rho_k\right)_{i+1/2}\left\lfloor -u_{k,i+1/2},0\right\rfloor \tag{83}$$

$$a_{k,i-1} = A_{i-1/2}\left(\alpha_k\rho_k\right)_{i-1/2}\left\lfloor u_{k,i-1/2},0\right\rfloor \tag{84}$$

$$\begin{aligned} b_{k,i} = {} & S_{k,i} + V_i\left[\frac{\left(\alpha_k\rho_k\right)^{t-\Delta t}_i h^{t-\Delta t}_{k,i}}{\Delta t} + K_{ik,i}h_{ksat,i} + \frac{K_{ik,i}}{8}\left(u_{k,i+1/2}+u_{k,i-1/2}\right)^2\right] \\ & + \frac{\left|S_{k,i}\right|h_{k,i}}{\Delta h_{k\max}} + \left[\Delta m_{k,i},0\right]h_{k,i} \end{aligned} \tag{85}$$

The following notations have been used in Equations (82) to (85):

$$S_{k,i} = V_i\left[\alpha_{k,i}\frac{p_i - p^{t-\Delta t}_i}{\Delta t} + \Gamma_k h_{ik,i} + F_{ik,i}u_{i,i} + \left(\alpha_k\rho_k\right)_i u_{k,i}\vec{g} + q_{wk,i}\right] \tag{86}$$

$$\begin{aligned} \Delta m_{k,i} = {} & V_i\frac{\left(\alpha_k\rho_k\right)_i - \left(\alpha_k\rho_k\right)^{t-\Delta t}_i}{\Delta t} + A_{i+1/2}\left(\alpha_k\rho_k\right)_{1+2}u_{k,i+1/2} \\ & - A_{i-1/2}\left(\alpha_k\rho_k\right)_{i-1/2}u_{k,i-1/2} - V_i\Gamma_{k,i} \end{aligned} \tag{87}$$

The quantity Δh_{max} means the maximum allowed change of enthalpy between consecutive iterations. The residual of the mass equation Δm corrects the effect of an erroneous mass balance.

4.5 Calculation of evaporating or condensing mass flow

The calculation of interfacial mass transfer is based on the requirement that the energy production of the interface is zero. Hence the following relationship is obtained:

$$\Gamma_i = -\frac{q_{i1,i} + q_{ig,i} - q_{wi,i}}{h_{g,sat} - h_{1,sat}} \tag{88}$$

where q_{wi} is the heat flowing from the wall directly to the interface.

The interfacial heat transfer rates are calculated as follows:

$$q_{i1,i} = -K_{i1,i}\left(h_{1,stat} - h_{1,sat}\right)_i \tag{89}$$

$$q_{ig,i} = -K_{ig,i}\left(h_{g,stat} - h_{g,sat}\right)_i . \tag{90}$$

The term Γ_i can change in some circumstances very rapidly and therefore it is linearized in the void fraction solution in respect to void fraction. The coefficients K_{ig} and K_{il} are usually dependent on the void fraction so for the linearization the following derivative is used:

$$\frac{\partial \Gamma}{\partial \alpha} = \left(\frac{h_{1,stat} - h_{1,sat}}{h_{g,sat} - h_{1,sat}}\right)\frac{\partial K_{i1}}{\partial \alpha} + \left(\frac{h_{g,stat} - h_{g,sat}}{h_{g,sat} - h_{1,sat}}\right)\frac{\partial K_{ig}}{\partial \alpha} . \tag{91}$$

In order to restrict rapid changes, also relaxation is employed in the calculation of mass transfer:

$$\Gamma^n = C\Gamma + \left(1 - C\right)\Gamma^{n-1} \tag{92}$$

where Γ is calculated from (88) and C is a relaxation factor between 0 and 1.

4.6 Critical mass flow rate

If the flow path is modeled accurately using a sufficient amount of nodes and branches, the solution system is supposed to limit the mass flows to the right level. However, it is sometimes necessary to use a special limitation (critical mass flow) to prevent the velocities from becoming too large.

When the pressure difference over a branch becomes very large, the critical mass flow limitation must be taken into account. In the critical flow model the flow is limited to correspond to the frozen velocity of the disturbance wave, i.e. interfacial mass transfer is assumed to be zero. The frozen sound velocity is calculated /2/

$$C_{fr} = \left[\frac{(1-\alpha)\rho}{\rho_1} \frac{1}{C_1^2} + \frac{1}{C_g^2} \right]^{1/2} \tag{93}$$

where the average density is calculated as follows:

$$\rho = \alpha\rho_g + (1-\alpha)\rho_1 . \tag{94}$$

The disturbance wave velocities of the two phases are related to the material properties in the following way:

$$\frac{1}{C_1^2} = \frac{\partial \rho_l}{\partial p} \tag{95}$$

$$\frac{1}{C_g^2} = \frac{\partial \rho_g}{\partial p} . \tag{96}$$

The average velocity of the flow is calculated as

$$\bar{u} = \frac{\alpha\rho_g u_g + (1-\alpha)\rho_1 u_1}{\rho} . \tag{97}$$

If the flow velocity $\bar{u} > C_{fr}$ the average velocity is set equal to the sound velocity

$$\bar{u} = C_{fr} . \tag{98}$$

In order to be able to utilize the term of Equation (98) the corresponding velocities u_g and u_l must be solved.

In case of the critical flow the flow is not dependent on the pressure gradient and therefore from Equations (43) the pressure differences $p_{i+1}^n - p_i^n$ can be eliminated. It is obtained

$$\left(b_g a_1 + b_1 c_g\right)u_i^n - \left(b_1 a_g + b_g c_1\right)u_g^n = b_g d_1 - b_1 d_g . \tag{99}$$

Equations (91) and (92) can be written in the form

$$H_g u_g + H_1 u_1 = C_{fr} . \tag{100}$$

When Equations (97) and (98) are solved together for u_g and u_l it is obtained

$$u_1 = \frac{\left(b_g c_1 + b_1 a_g\right)C_{fr} + H_g\left(b_g d_1 - b_1 d_g\right)}{H_g\left(b_g a_1 + b_1 c_g\right) + H_1\left(b_1 a_g + b_g c_1\right)} \tag{101}$$

$$u_g = \frac{C_{fr}}{H_g} - \frac{H_1}{H_g} u_1 . \tag{102}$$

If the critical flow is exceeded, the velocities are calculated using Equations (101) and (102). In the pressure equation the coefficient U_k is set to u_k and D_k is set to zero.

4.7 Solution of boron concentrations

Boron is assumed to stay only in the liquid phase and hence the concentration equation is

$$\frac{\partial\left(1-\alpha\right)\rho_1 x_b}{\partial t} + \frac{\partial\left(1-\alpha\right)\rho_1 u_1 x_b}{\partial z} = 0 . \tag{103}$$

The concentration equation is discretized in the same manner as the corresponding terms of the energy equation. The first term becomes

$$V_i \frac{\left(1-\alpha_i\right)\rho_{1,i} x_{b,i}^n - \left[\left(1-\alpha\right)\rho_1 x_{b.i}\right]^{t-\Delta t}}{\Delta t} . \tag{104}$$

In the discretization of the second term the upwind values are used for concentration, hence it is obtained

$$
\begin{aligned}
&A_{i+1/2}\left[(1-\alpha)\rho_1\right]_{i+1/2}\left[u_{1,i+1/2},0\right]x^n_{b,i} \\
&-A_{i-1/2}\left[(1-\alpha)\rho_1\right]_{i\text{-}1/2}\left[u_{1,i-1/2},0\right]x^n_{b,i-1} \\
&-A_{i-1/2}\left[(1-\alpha)\rho_1\right]_{i\text{-}1/2}\left[-u_{1,i-1/2},0\right]x^n_{b,i} \\
&-A_{i+1/2}\left[(1-\alpha)\rho_1\right]_{i+1/2}\left[-u_{1,i+1/2},0\right]x^n_{b,i+1}
\end{aligned}
\tag{105}
$$

Finally, the following equation for the concentration solution is obtained:

$$
a_i x^n_{b,i} = a_{i+1}x^n_{b,i+1} + a_{i-1}x^n_{b,i-1} + b_i \tag{106}
$$

where

$$
\begin{aligned}
a_i = {} & A_{i+1/2}\left[(1-\alpha)\rho_1\right]_{i+1/2}\left[u_{1,i+1/},0\right] \\
& + A_{i-1/2}\left[(1-\alpha)\rho_1\right]_{i-1/2}\left[-u_{1,i-1/},0\right] + V_i\,\frac{\left[(1-\alpha)\rho_1\right]_i}{\Delta t}
\end{aligned}
\tag{107}
$$

$$
a_{i+1} = A_{i+1/2}\left[(1-\alpha)\rho_1\right]_{i+1/2}\left[-u_{1,i+1/},0\right] \tag{108}
$$

$$
a_{i\text{-}1} = A_{i\text{-}1/2}\left[(1-\alpha)\rho_1\right]_{i\text{-}1/2}\left[u_{1,i\text{-}1/},0\right] \tag{109}
$$

$$
b_i = V_i\,\frac{\left[(1-\alpha)\rho_1\right]^{t-\Delta t}_i x^{t-\Delta t}_{b,i}}{\Delta t}. \tag{110}
$$

Because it is assumed that boron has no effect on the flow conditions, the concentration solution is made after the pressure, void fraction, non-condensable gas density and enthalpy solutions have converged.

4.8 Boundary conditions

Boundary conditions can be defined using external nodes and branches. The pressures, enthalpies, void fractions and boron concentrations stay constant in external nodes. The material properties are calculated from the pressures and enthalpies. During the simulation, the external nodes contribute to the solution in the adjacent nodes according to the equations of the previous sections.

The velocities stay constant in external branches. In order to eliminate the coupling of the pressure and flow solutions, the coefficients normally used in the velocity calculation in Equation (44) are changed to:

$$D_{k,i+1/2} = 0$$
$$U_{k,i+1/2} = u_{k,i+1/2} \tag{111}$$

The velocities of the external branches are used in the other solutions analogously to the velocities of the normal branches. A constant mass flow into the system can be defined by combining an external node and an external branch.

A branch between a node of some other accuracy level (homogeneous model or 5 equation model) and a level 6 node is treated using an external branch and an external node. The model of the other level solves the flow in a connecting branch using the level 6 pressure as a pressure boundary. Then the calculated mass flow is used as a mass flow boundary condition for level 6. The momentum change $\Delta\left(A\alpha_k\rho_k u_k^2\right)$ of the level 6 branch connecting different accuracy levels is set to zero.

5. Friction and heat transfer correlations

The solution of six-equation model requires that the quantities solved with aid of six partial differential equations are coupled together. For this purpose the empirical correlations are used. The six equation model requires correlations for interfacial friction and interfacial heat transfer. The wall friction and wall heat transfer have to be calculated for both liquid and steam.

The phenomena which depend on the transverse gradients, like friction and heat transfer between the gas and liquid phases and between the wall and both phases, have been described with empirical correlations. The correlations are strongly dependent on the flow regime and different correlations are usually used for different flow regimes. The flow regimes which are treated in the code are bubbly, annular, droplet and stratified flows. In the calculations, the real prevailing flow mode usually consists of more than one individual flow regime. When the correlations are applied, the different flow regimes are taken into account by the weighting factors.

5.1 Auxiliary variables

In order to calculate the friction and heat transfer terms, several auxiliary variables are needed in addition to those calculated as a function of pressure and enthalpy in the material property table program. The surface tension is calculated as a function of liquid temperature:

$$\sigma = c_1 T_1 + c_2 \tag{112}$$

where the constants are c_1 = -2·10^{-4} N/m°C and c_2 = 0.075 N/m. The function is derived from the tabulated values of surface tension /3/.

The droplet diameter is a very important quantity. It determines the size of the interface of the two phases and greatly affects interfacial friction and heat transfer. The diameter is calculated from the formula /4/

$$\delta = \min\left(\frac{8\sigma}{\rho_g (\Delta u)^2}, 1.73 \sqrt{\frac{\sigma}{g(\rho_1 - \rho_g)}} \right). \tag{113}$$

The Reynolds number is a dimensionless quantity which can be calculated for each phase and a single droplet. The definition of the Reynolds number of phase k is

$$\mathrm{Re}_k = \frac{\alpha_k \rho_k |u_k| D}{\eta_k}. \tag{114}$$

The droplet Reynolds number is calculated using gas properties, diameter of a droplet and the velocity difference between the phases:

$$\mathrm{Re}_d = \frac{\rho_g |\Delta u| \delta}{\eta_g}. \tag{115}$$

The Prandtl number of phase *k* is calculated from the formula

$$\mathrm{Pr}_k = \frac{\eta_k c_{pk}}{\lambda_k}. \tag{116}$$

The rate of entrainment means the fraction of the liquid phase existing in droplets and it is calculated as follows:

$$E = \left(1 - \frac{1.8 \cdot 10^{-4}}{\pi}\right)^2 \cdot f(\alpha) \tag{117}$$

where

$$\pi = \frac{\alpha |u_g| \eta_g}{\sigma} \sqrt{\frac{\rho_g}{\rho_1}}. \tag{118}$$

The formula is an approximation of the data given in /5/. The function *f* restricts the droplet flow at low void fractions.

The mass fraction of the gas phase is calculated from the void fractions and densities as follows:

$$X = \frac{\alpha \rho_g}{\alpha \rho_g + (1-\alpha)\rho_1}. \tag{119}$$

The mass flux of the mixture is calculated as

$$G = \alpha \rho_g u_g + (1-\alpha)\rho_1 u_1. \tag{120}$$

5.2 Wall friction

Wall friction for both phases is calculated using the formula

$$F_{wk} = \frac{-2C_{wk}\rho_k u_k |u_k|}{D}. \tag{121}$$

One phase friction coefficients are calculated using the turbulent formula (Blasius) and laminar formula. The final friction coefficients of phases are calculated using the void fraction as s weighting factor. For gas the friction coefficient is

$$C_{wg} = \alpha^5 \cdot \max\left(\frac{16}{\mathrm{Re}_g}, 0.079\,\mathrm{Re}_g^{-1/4}\right) \tag{122}$$

and for liquid the coefficient is

$$\mathrm{C_{w1}} = \left(1-\alpha^5\right)\cdot \max\left(\frac{16}{\mathrm{Re}_1}, 0.079\mathrm{Re}_1^{-1/4}\right). \tag{123}$$

The term depending on void fraction approximates the fraction of each phase on the wall.

5.3 Interfacial friction

Interfacial friction is calculated from three different correlations. They describe three types of flow: bubbly flow (low void fractions), annular flow (high void fractions) and droplet flow (high void fractions, liquid is in the form of droplets). The final value of interfacial friction is obtained as a weighted average of the correlations:

$$F_i = (1-E)\left[(1-\alpha)F_{ib} + \alpha F_{ia}\right] + EF_{id}. \tag{124}$$

The interfacial friction of bubbly flow is /4, 6/

$$F_{ib} = \left(\frac{29\rho_g}{L} + \frac{f_L F_{\eta l}^{1/4}\rho_1}{D}\right)\alpha(1-\alpha)^3 \Delta u|\Delta u| \tag{125}$$

where

$$L = \left(\frac{1}{D^2} + \frac{g\left(\rho_1 - \rho_g\right)}{f^2 \sigma} \right)^{-1/2} \tag{126}$$

$$\begin{aligned} f &= 1.3 + 15.7\alpha^3\left(256 - 768\alpha\right), \; if \;\; \alpha < 0.25 \;\; or \\ f &= 17, \qquad\qquad\qquad\qquad if \;\; \alpha \geq 0.25 \end{aligned} \tag{127}$$

$$f_L = 2.81 + 34\left(\frac{L}{D}\right)^5 \left(6 - \frac{5L}{D}\right) \tag{128}$$

$$F_{\eta k} = \eta_k \left[\frac{g\left(\rho_1 - \rho_g\right)}{\rho_k^2 \sigma^3} \right]^{1/4} . \tag{129}$$

In annular flow the interfacial friction is calculated as follows /2/:

$$F_{ia} = \frac{0.01\left[1 + 75\left(1 - \alpha\right)\right]\rho_g \Delta u \left|\Delta u\right|}{D} . \tag{130}$$

The interfacial area is proportional to the droplet diameter in droplet flow and interfacial friction is calculated from the formula /4/

$$F_{id} = \frac{0.75\left(1 - \alpha\right) C_i \rho_g \Delta u \left|\Delta u\right|}{\delta} . \tag{131}$$

The friction coefficient C_i depends on the Reynolds number of droplet:

$$C_i = \frac{24}{\mathrm{Re}_d} + \frac{3.6}{RE_d^{0.313}} + \frac{0.42}{1 + 4.25 \cdot 10^4 \cdot \mathrm{Re}_d^{-1.16}} . \tag{132}$$

5.4 Interfacial heat transfer

The interfacial heat transfer in two-fluid model has to be calculated separately for the liquid and gas.

For the gas, when the vapour is subcooled, the interfacial heat transfer coefficient is calculated from the Lee-Ryley correlation /7/:

$$K_{ig} = \frac{6(1-\alpha)\lambda_g\left(2 + 0.74 RE_d^{1/2}\,\mathrm{Pr}_g^{1/3}\right)}{\delta^2 c_{pg}} \qquad \text{if } h_{g,stat} < h_{g,sat} \tag{133}$$

The coefficient is reduced in vaporization /4/:

$$K_{ig} = \frac{6(1-\alpha)\lambda_g\left(2 + 0.74\,\mathrm{Re}_d^{1/2}\,\mathrm{Pr}_g^{1/3}\right)}{\delta^2 c_{pg}} \cdot \frac{1}{1 + 10^{-3}\left(T_g - T_{sat}\right)} \qquad \text{if } h_{g,stat} > h_{g,sat} \tag{134}$$

The interfacial heat transfer coefficient of the liquid phase is calculated as follows in vaporization /8/:

$$K_{il} = \frac{1.2 \cdot 10^{-8} \cdot \exp(4.5\alpha)\rho_1^2 u_1^2}{\eta_l\,\mathrm{Pr}_l} \qquad \text{if } h_{l,stat} > h_{l,sat} \tag{135}$$

The Shah correlation /9/ is used in condensation. The heat transfer coefficient is increased in droplet flow /4/:

$$K_{il} = \frac{0.092\ \mathrm{Re}_1^{0.8}\,\mathrm{Pr}_1^{0.4}\,\lambda_1}{D^2 c_{pl}} \cdot \left[(1-x)^{0.8} + 3.8x^{0.76}(1-x)^{0.04}\left(\frac{P_{cr}}{P}\right)^{0.38}\right] + E \cdot \frac{6(1-\alpha)\lambda_1}{\delta^2 c_{pl}} \qquad \text{if } h_{l,stat} < h_{l,sat} \tag{136}$$

where p_{cr} is critical pressure (22.064 MPa).

5.5 Wall heat transfer

There are three separate heat transfer zones where the wall heat transfer is calculated from different correlations: wetted wall, dry wall and a transition zone between wetted and dry wall. If the wall temperature is lower than the saturation temperature of the fluid, only water is assumed to be in contact with the wall. When the wall temperature rises, the heat flux increases. After the heat flux has exceeded the critical heat flux, the wall begins to dry out and the heat transfer decreases (see Figure 1). The transition zone ranges from the critical heat flux temperature T_{CHF} to the minimum film boiling

temperature T_{MFB} above which there is only gas on the wall and the heat flux begins to increase again. During rewetting the wall temperature decreases and the wall changes from dry to wet.

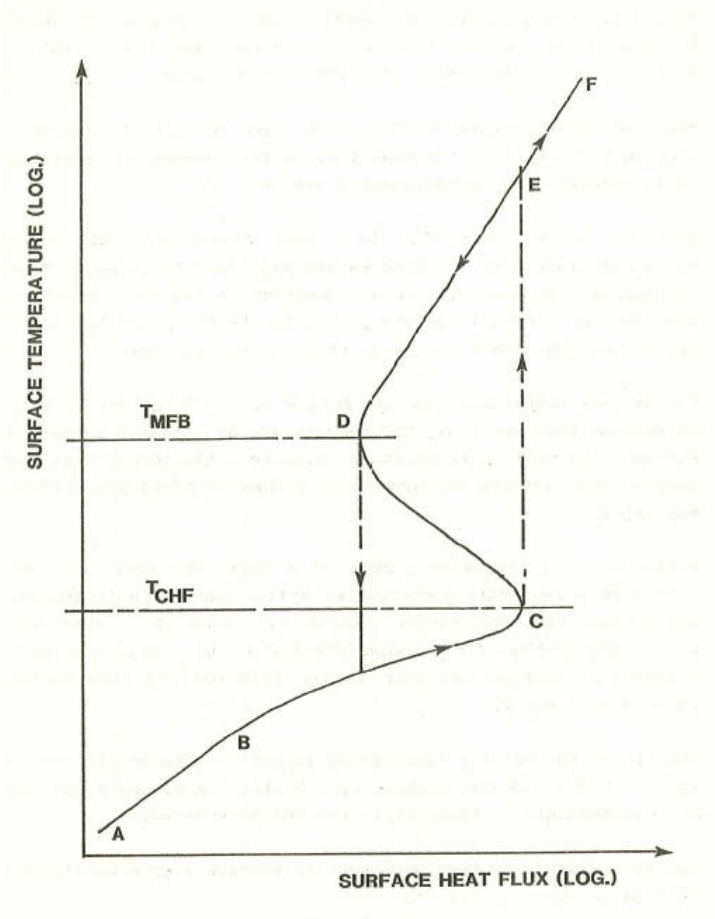

Figure 1. Heat transfer zones /10/.

The heat transfer zone changes from wet to the transition zone, if the wall temperature T_w is greater than the saturation temperature T_{sat} and if the heat flux $Q = Q_{wl} + Q_{wg} + Q_{wi}$ is greater than the critical heat flux Q_{cr}. The change to the wet zone happens, when the wall temperature drops below the saturation temperature. The border of the transition zone and the dry zone is determined by the minimum film boiling temperature. The total heat flux is obtained by adding the radiation heat fluxes $Q_{l,rad}$ and $Q_{g,rad}$ to Q. Radiation heat transfer is calculated with the Deruaz-Petitpain model /11/. The heat flux is converted to specific heat flow q by multiplying with the surface area of the heat structure node and dividing with the volume of the hydraulic node.

5.5.1 Critical heat flux

The critical heat flux is calculated from the Zuber-Griffith correlation on low flows and otherwise from the Biasi correlation /12/:

$$Q_{cr} = 0.131(1-\alpha)\rho_g\left(h_{g,sat} - h_{l,sat}\right)\left[\frac{\sigma g\left(\rho_l - \rho_g\right)}{\rho_g^2}\right]^{1/4} \qquad (137)$$

$$\text{if } |G| \le 100\, kg/m^2 s$$

$$Q_{cr} = \max\left\{\frac{1.883\cdot 10^7}{(100D)^n\left(|G|/10\right)^{0.167}}\left[\frac{f}{\left(|G|/10\right)^{0.167}} - x\right], \frac{3.89\cdot 10^7}{(100D)^n\left(|G|/10\right)^{0.6}}h(1-x)\right\} \qquad (138)$$

$$if\ |G| \ge 200\, kg/m^2 s$$

where

$$n = 0.4\ ,\ \text{if } D \ge 0.01m \quad \text{or}$$
$$0.6\ ,\ \text{if } D < 0.01m$$

$$f = 0.7249 + 9.9\cdot 10^{-7}\, p\cdot\exp\left(-3.2\cdot 10^{-7}\, p\right)$$

$$h = -1.159 + 1.49\cdot 10^{-6}\, p\cdot\exp\left(-1.9\cdot 10^{-7}\, p\right) + \frac{9\cdot 10^{-5}\, p}{10 + 10^{-10}\, p^2}\ .$$

When the mass flux is between 100 and 200 kg/m^{2}s, the critical heat flux is interpolated between the two correlations.

5.5.2 Heat transfer on a wetted wall

The heat flux on a wetted wall is calculated from the Dittus-Boelter correlation for forced convection and the Thom correlation for nucleate boiling /12/. The switching to nucleate boiling occurs when the wall temperature exceeds the saturation temperature of the fluid. In nucleate boiling, the flux is distributed between the liquid phase and the interface. The distribution factor is a function of the liquid subcooling.

$$Q_{wl} = \frac{0.023\,\mathrm{Re}_1^{0.8}\,\mathrm{Pr}_1^{0.4}\,\lambda_1}{D}\left(T_w - T_l\right) \qquad (139)$$

$$\text{if } T_w \le T_{sat} \text{ and wetted wall}$$

$$Q_{wl} + Q_{wi} = 1970 \cdot \exp\left(2.3 \cdot 10^{-7}\, p\right)\left(T_w - T_{sat}\right)^2 \quad \text{if } T_w > T_{sat} \text{ and wetted wall} \tag{140}$$

5.5.3 Heat transfer on a dry wall

The heat transfer correlations of a dry wall are used when the wall temperature is greater than the minimum film boiling temperature. The minimum film boiling temperature is calculated with the Groeneveld-Stewart correlation /12/:

$$T_{MFB} = 284.7\,^{o}C + 4.41 \cdot 10^{-5}\, p - 3.72 \cdot 10^{-12}\, p^2 - \frac{10^4\left(h_{l,stat} - h_{l,sat}\right)}{\left(2.82 + 1.22 \cdot 10^{-6}\, p\right)\left(h_{g,sat} - h_{l,sat}\right)} \quad \text{if } p \le 9 \cdot 10^6\ Pa \tag{141}$$

and

$$T_{MFB} = \left[T_{MFB}\left(p = 9 \cdot 10^6\ Pa\right) - 303\,^{o}C\right] \frac{p_{cr} - p}{p_{cr} - 9 \cdot 10^6\ Pa} + T_{sat} \quad \text{if } p > 9 \cdot 10^6\ Pa \tag{142}$$

where $T_{MFB}(p=9 \cdot 10^6$ Pa) is calculated from formula (133) and 303 °C is the saturation temperature at the pressure $9 \cdot 10^6$ Pa.

The heat flux between a dry wall and the gas phase is calculated as follows /4/:

$$Q_{wg} = \max\left(K_{wg1}, K_{wg2}, K_{wg3}, K_{wg4}\right)\left(T_w - T_g\right) \tag{143}$$

The heat transfer coefficient K_{wg1} is the Berenson coefficient for pool boiling, K_{wg2} and K_{wg3} correspond to laminar and turbulent forced convection and K_{wg4} is the heat transfer coefficient of natural convection. The Dittus-Boelter correlation is used for forced convection. The coefficients are calculated from the following formulas:

$$K_{wg1} = 0.425\left[\frac{\lambda_g^3\, \rho_g\, g^{3/2}\left(\rho_l - \rho_g\right)^{3/2}\left(h_{g,sat} - h_{l,sat}\right)}{\eta_g\left(T_w - T_g\right)\sigma^{1/2}}\right]^{1/4} \cdot \sqrt{1-\alpha}\ \left[1 + 0.025\left(T_{sat} - T_l\right)\right] \tag{144}$$

$$K_{wg2} = \frac{3.66\,\lambda_g}{D_g} \tag{145}$$

$$K_{wg3} = \frac{0.023\,\lambda_g}{D_g}\left[\frac{\rho_g |u_g| D_g}{\eta_g}\right]^{0.8} \mathrm{Pr}_g^{0.4} \tag{146}$$

$$K_{wg4} = \frac{\lambda_g}{D_g} \cdot \max\left(0.401\,Gr_g^{1/4}\,\mathrm{Pr}_g^{1/4},\, 0.12\,Gr_g^{1/3}\,\mathrm{Pr}_g^{1/3}\right). \tag{147}$$

The thickness of the gas film is a function of void fraction:

$$D_g = D\left(1 - \sqrt{1-\alpha}\right). \tag{148}$$

The Grashof number is defined as

$$Gr_g = \frac{g\,\rho_g^2\,D_g^3 |T_w - T_g|}{\eta^2 \left(T_g + 273.15)\right)}. \tag{149}$$

In the transition zone between wetted and dry wall, the heat flux is interpolated between the critical heat flux and the heat flux from dry wall /4/. The part of the heat flux due to the critical heat flux is distributed between the liquid phase and interface in the same way as in nucleate boiling.

5.5.4 Rewetting

Rewetting occurs when part of the system is in the wet heat transfer zone and part in the dry zone. The quench front height is the height of the boundary between the wetted and dry regions. Because droplets are ejected near the quench front and the flow is agitated, the heat transfer above the quench front is increased. The additional heat flux is calculated as follows /4/:

$$Q = \max\left(1 - \frac{h - h_{qf}}{0.745},\, 0\right)\left[1400(1-\alpha)(T_w - T_{sat}) + K\frac{\partial T_w}{\partial z}\right] \tag{150}$$
$$if\ \ h > h_{qf}$$

The coefficient K depends on pressure, mass flux and the mass fraction of gas /13/.

Smaller droplets than normally are generated above the quench front, and formula (113) is modified by limiting the droplet size according to Equation (151):

$$\delta = \min\left(\frac{8\sigma}{\rho_g (\Delta u)^2}, 0.54\sqrt{\frac{\sigma}{g(\rho_l - \rho_g)}} \right) \quad \text{if } h > h_{qf} \tag{151}$$

6. Test cases

The two-phase model has been tested by calculating several well-known test cases. The calculation of these tests is repeated every time new version of APROS is released. The current calculations are carried out with version 5.08. The calculation results agree fairly well with the measured data in all cases.

6.1 Edwards pipe

The so-called Edwards pipe /14/ is a horizontal pipe, which is closed in the beginning of the test and contains water under high pressure (6.895 MPa). The initial water temperature is 242 °C. The length of the pipe is 4.096 m and diameter 0.073 m (see Figure 2). The head of the pipe is punctured, after which water begins to evaporate and flow out of the tube with a great velocity. The pressure in the pipe decreases rapidly in the beginning, then follows an almost horizontal phase and after about 0.25 seconds the drop becomes steeper until the pressure finally drops to the air pressure.

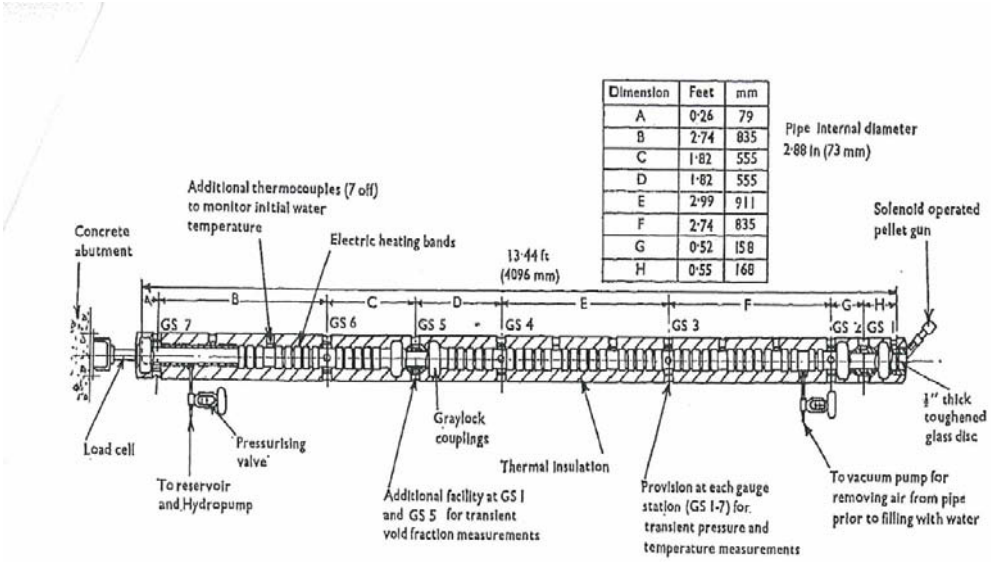

Figure 2. Edwards pipe test facility /14/.

The calculated pressures follow the measured trends quite well (see Figures 3 and 4), although the final decrease begins too early. The start point of the pressure decrease in the closed end node has been well predicted (Figure 5). The test has been simulated by dividing the pipe into 50 nodes. If only a few nodes are used, the results differ a little more from the measurements. The increasing of the number of nodes over 50 does not change the results significantly.

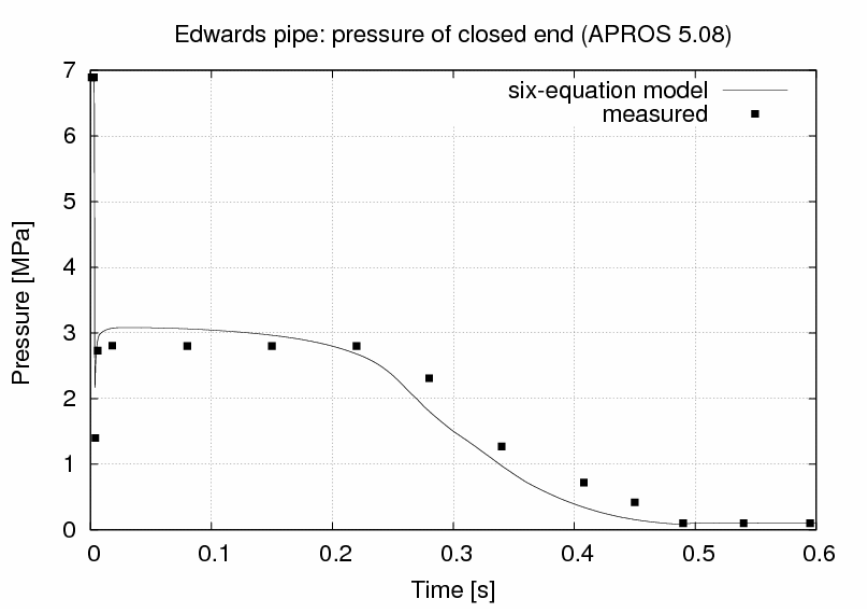

Figure 3. Pressure in the closed end of Edwards pipe (continuous line: 50 calculation node, dots: measurement data).

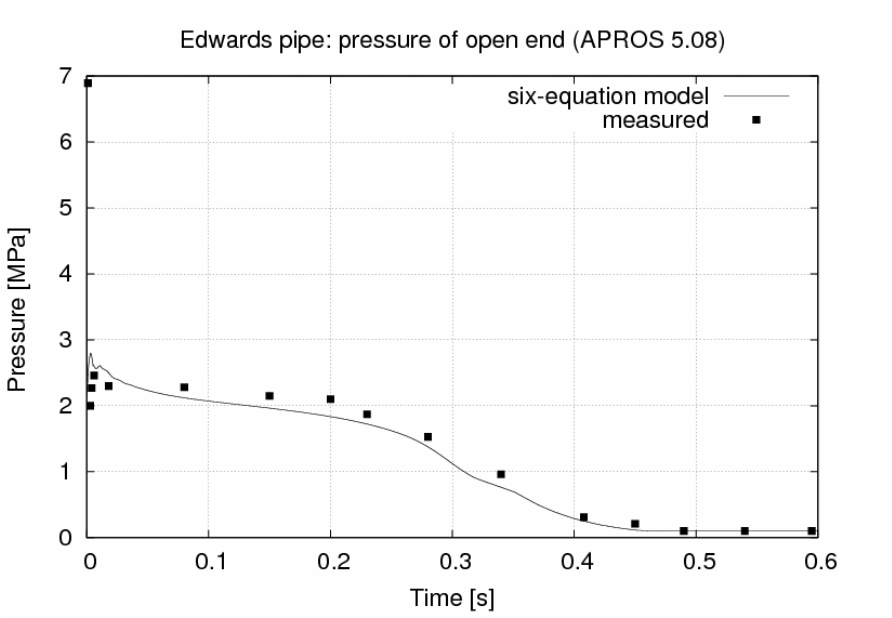

Figure 4. Pressure in the open end of Edwards pipe (continuous line: 50 calculation nodes, broken line: 10 calculation nodes, circles: measurement data).

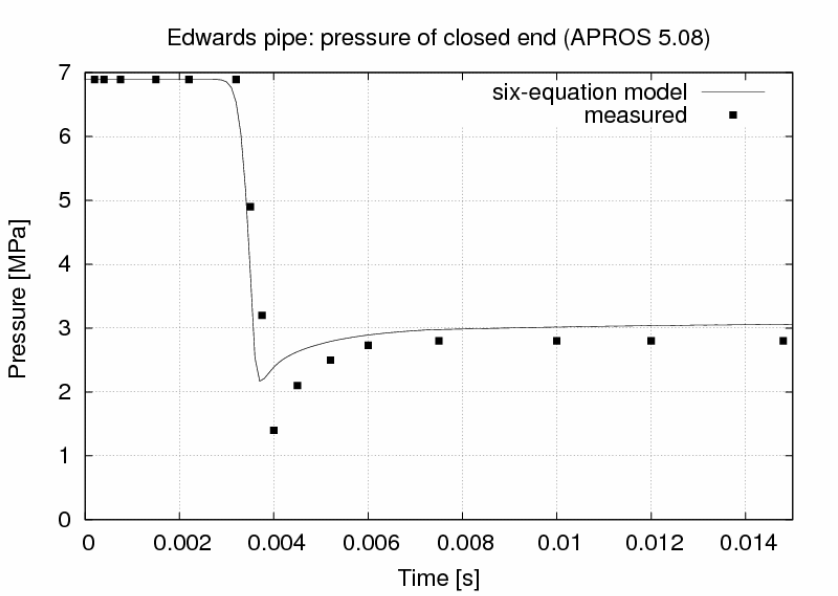

Figure 5. Pressure in the closed end of Edwards pipe at the first part of transient (continuous line: 50 calculation node, dots: measurement data).

6.2 Top blowdown experiment

The second test case is a top blowdown experiment (OECD Standard Problem No. 6) /15/. This experiment demonstrates the rise of water level in a boiling water reactor in case when the pressure is suddenly decreased. The test vessel has an inner diameter of 0.77 m and a height of 11.19 m (see Figure 6). The initial pressure is 7.07 MPa, temperature 285 °C and height of water level 7.07 m. In the beginning of the test a break orifice in the discharge nozzle (at the height of 10.01 m) is opened. The area of the orifice is 0.064 m. The nozzle is modeled with a small node. The branches coming to and leaving from the node have suitable loss coefficients in order to acquire the correct mass flow in the beginning.

When the break orifice is opened, the water level begins to rise. When the level rises to the discharge height, the break flow (the sum of the mass flows of water and steam) increases sharply because of liquid discharge. The calculated mass flow begins to increase almost at the right time and the maximum flow is a little higher than in the measurements. The more calculation nodes are used, the sharper the increase is obtained (Figure 7).

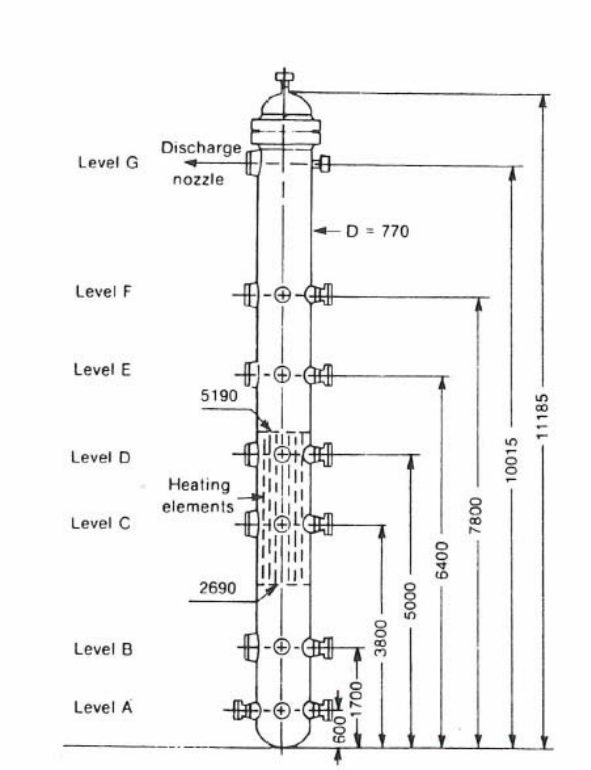

Figure 6. Test facility of the top blowdown experiment /15/.

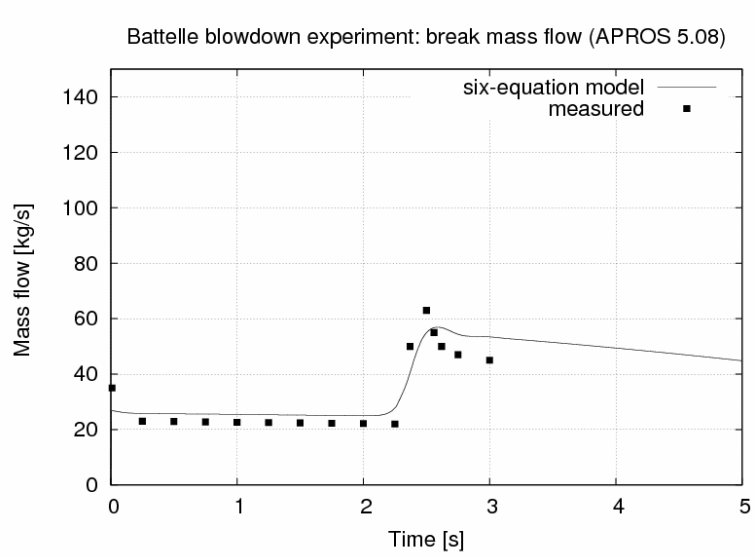

Figure 7. Break mass flow in the top blowdown experiment (continuous line: calculated values with Δz = 0.05 m, dots: measurement data).

6.3 Becker experiments

The Becker experiments /10/ have been used to test the heat transfer correlations for dry out and post dry out at steady state conditions. The test section is a vertical tube filled with water in the beginning of the test. The wall of the tube is directly heated with a

uniform power distribution and insulated on the outer surface. The inside diameter of the tube is 0.0149 m and the heated length 7 m. Water flows into the system at a constant rate from below.

The experiments have been calculated by dividing the tube into 100 nodes and into corresponding number of heat structures. The boundary conditions were defined by an external branch with the desired mass flow into the system and an external node with the correct exit pressure. The tests were carried out by simulating the system until it reached a steady state. This took about 50–100 seconds of simulation time. The wall temperature distribution at different heights corresponding to calculated three cases can be seen in Figures 8, 9 and 10. In case 1, the pressure was 5.02 MPa, incoming mass flux 1476 kg/m^{2}s, the subcooling of the inflowing water 9.8 °C and the heat generation rate 1.015 MW/m^2. The corresponding values in case 2 were 10.01 MPa, 502 kg/m^{2}s, 12.1 °C and 0.457 MW/m^2. In the third case pressure was 2.98 MPa, inflow mass flux was 498 kg/m^{2}s, subcooling 8.9 ºC and heat rate 0.562 MW/m^2.

A dry out phenomenon occurs in the upper part of the tube, i.e. the heat flux exceeds the critical heat flux. A sharp increase in the wall temperature distribution is noticed on the border of wetted and dry wall. The height of the border in the calculation results is quite close to the measurements. However, the shape of the distribution differs somewhat above the border. The point for the dry out position was difficult to predict. In case 3 the position was well calculated, but in case 1 and 2 the calculated the dry out occurred clearly too late. In the present calculation the critical heat flux was simulated with Biasi correlation.

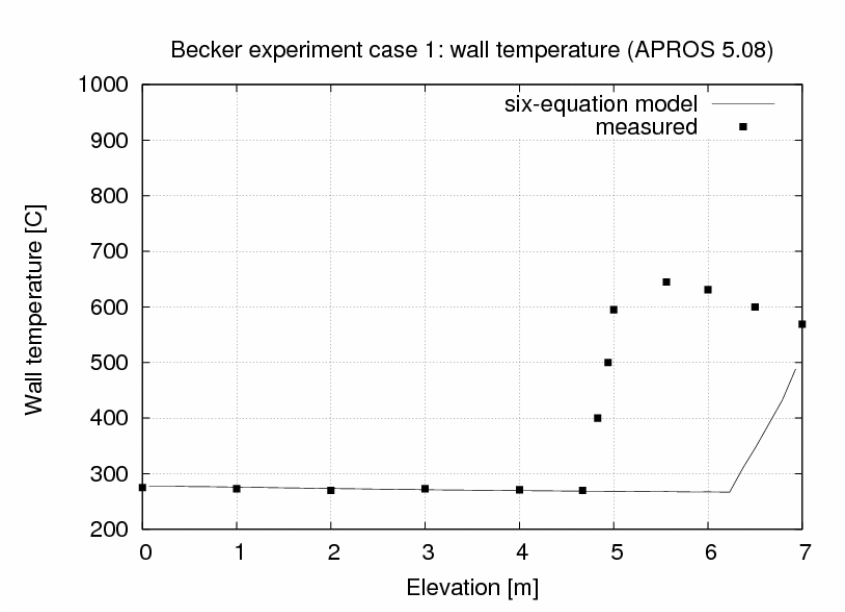

Figure 8. The wall temperatures at different elevations in case 1 of the Becker experiments (continuous line: calculated values, dots: measurement data).

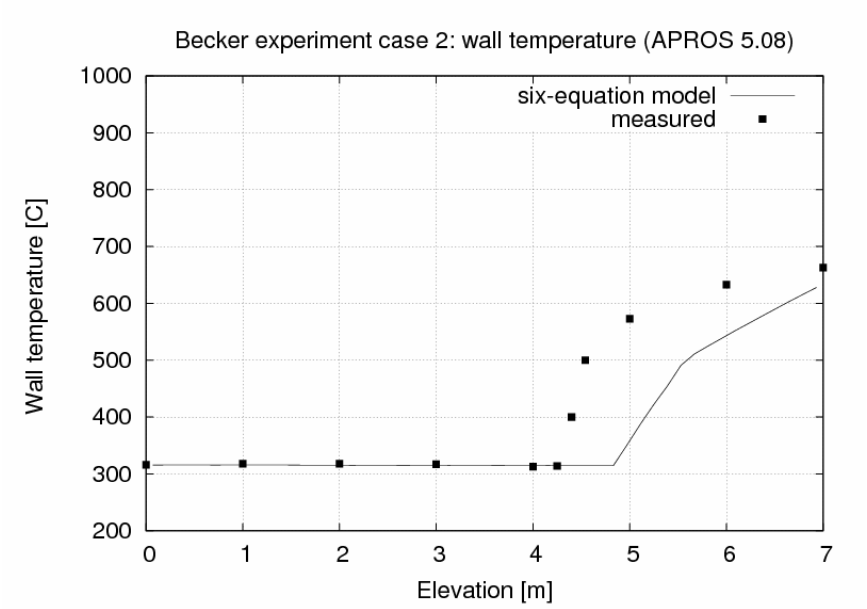

Figure 9. The wall temperatures at different elevations in case 2 of the Becker experiments (continuous line: calculated values, dots: measurement data).

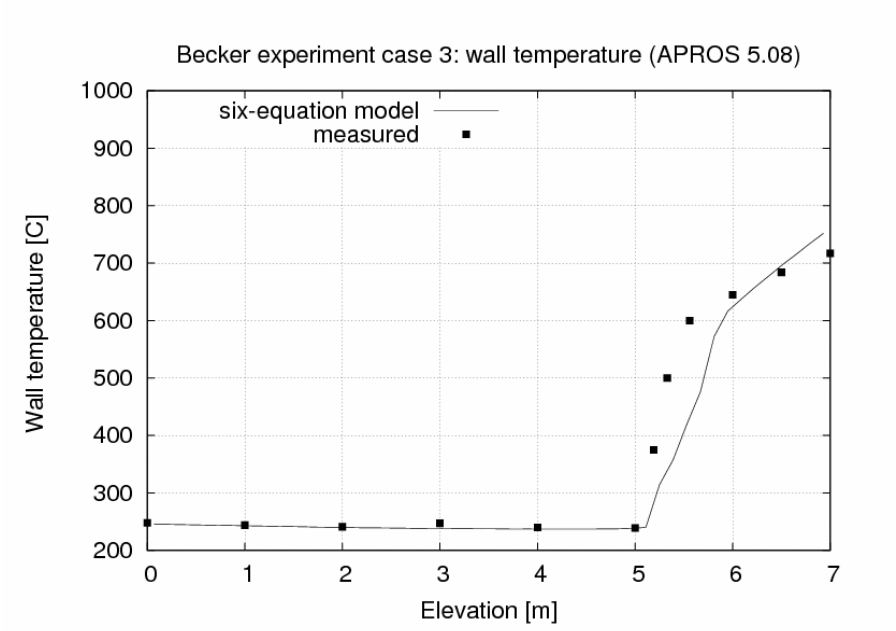

Figure 10. The wall temperatures at different elevations in case 3 of the Becker experiments (continuous line: calculated values, dots: measurement data).

6.4 Rewetting experiment

The seventh CSNI Standard Problem on LOCA /16/ is an experiment where rewetting occurs. The test facility is a vertical, uniformly heated tube (see Figure 11). It is filled with steam (pressure 3 bars) in the beginning. Water flows into the tube with a constant

rate of 52 kg/m^{2}s and a subcooling of 23 °C. The heat generation in the whole tube is 6267.5 W. The tube is made of Inconel 600 and has an inner diameter of 12 mm, outer diameter 14 mm and length 3.325 m.

The test is modeled by a pipe divided into 100 nodes. A moving heat structure mesh is applied so that the tube is cut axially into 1 mm long heat structure nodes where the temperature gradient is greatest. Elsewhere, there is one heat structure for each hydraulic node. The heat conduction is solved by a two-dimensional model (radial and axial conduction).

The calculated wall temperatures follow the shape of the measured data quite well (Figures 12 and 13). However, the calculated position of the quench front moves too quickly in the beginning of the test and too slowly in the end, which can be observed in the quenching front propagation curve (Figure 14). Finally, the whole tube has been wetted. This occurs about 200 seconds too late in the simulation.

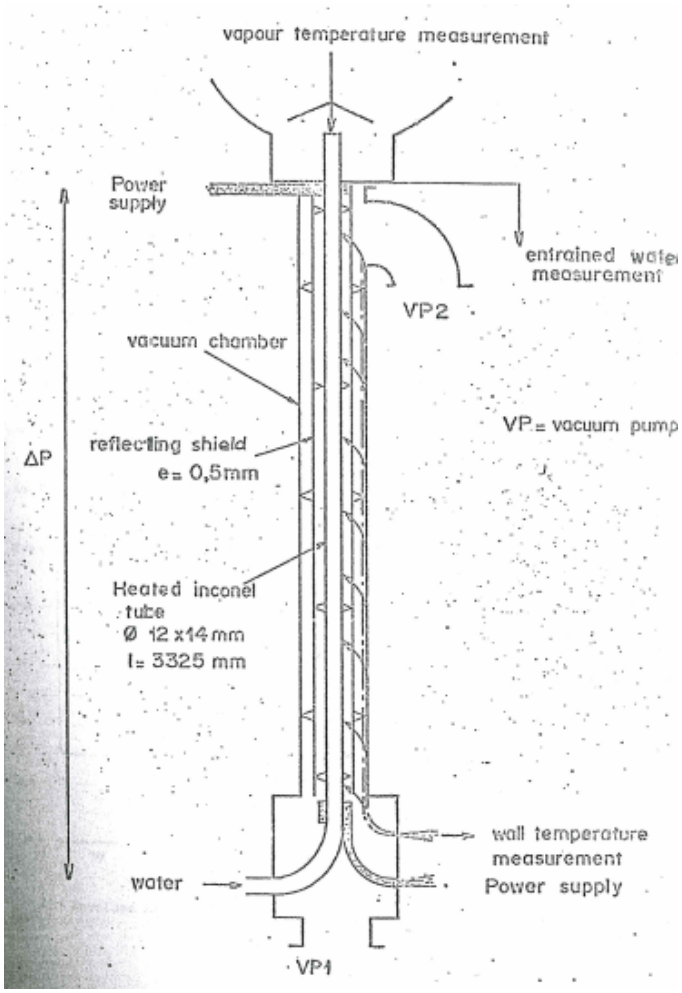

Figure 11. Test facility of the seventh CSNI Standard Problem on LOCA /16/.

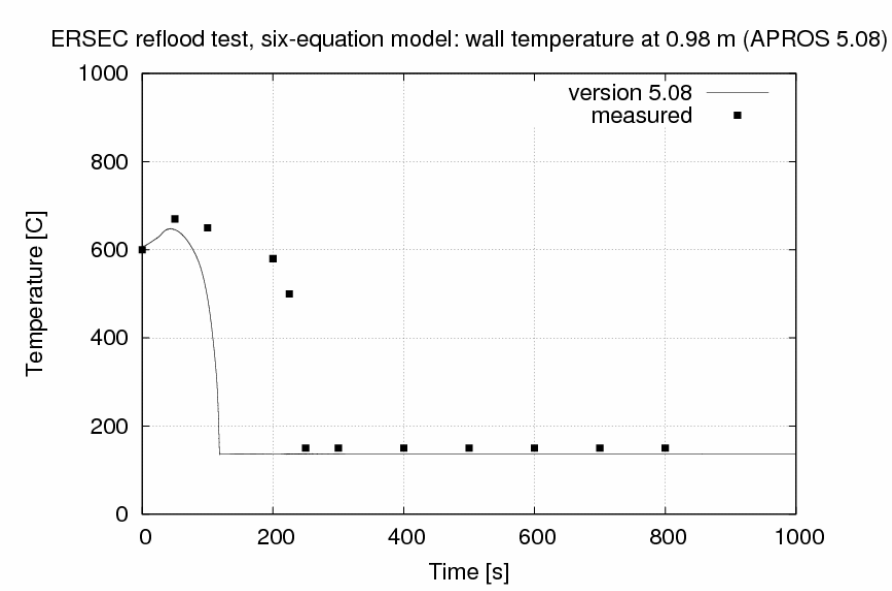

Figure 12. Wall temperature at the elevation of 0.98 m in the seventh CSNI Standard Problem on LOCA (continuous line: calculated values, dots: measurement data).

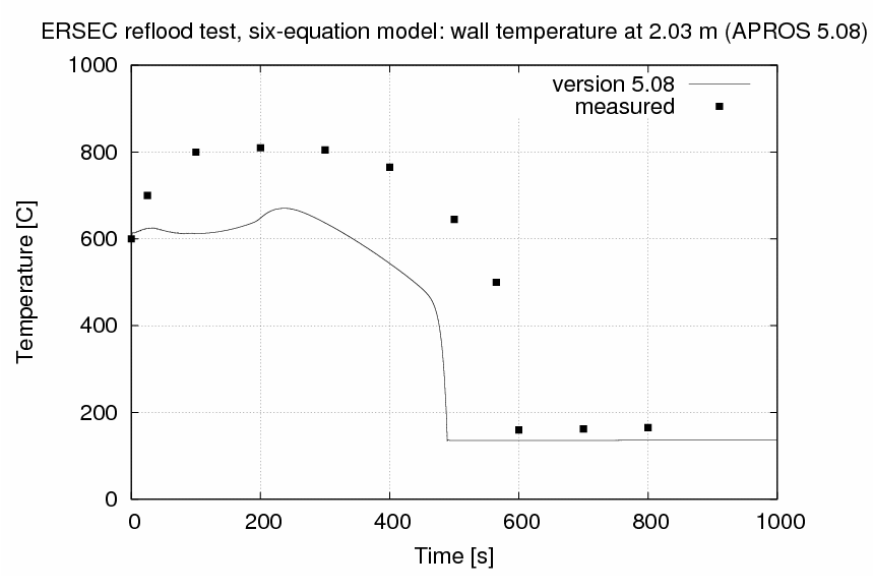

Figure 13. Wall temperature at the elevation of 2.03 m in the seventh CSNI Standard Problem on LOCA (continuous line: calculated values, dots: measurement data).

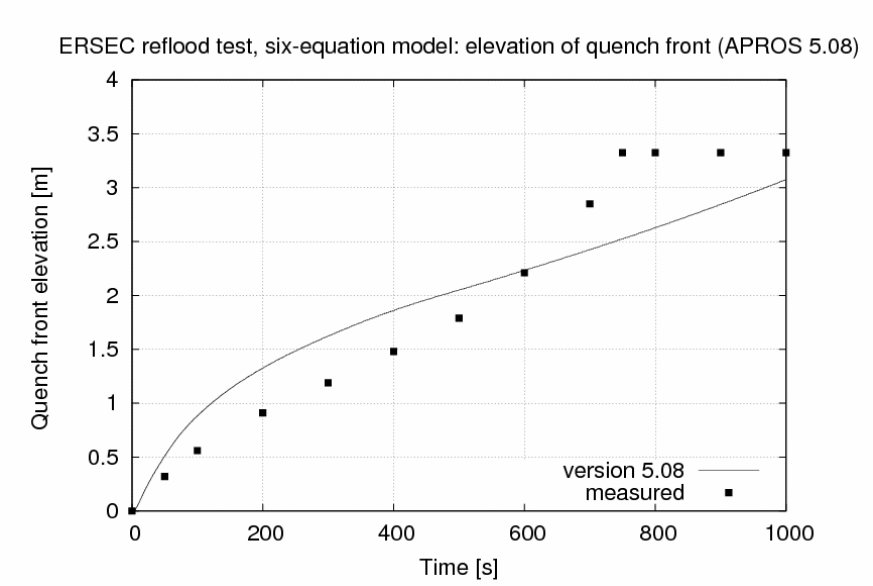

Figure 14. The elevation of the quench front in the seventh CSNI Standard Problem on LOCA (continuous line: calculated values, dots: measurement data).

7. Conclusions

The one-dimensional separate two-phase flow model of APROS has been described. The derivation of the calculation model from the governing differential equations has been shown in detail. Also the friction and heat transfer correlations for wall and interface used to close the set of the linear equations have been briefly presented. The derived linear equation groups for pressures, enthalpies, void fractions, non-condensable gas densities and boron concentrations are solved by the matrix equation solver and the final solution is searched iteratively. The flow velocities can be solved directly after the pressure solution.

The two-phase model is connected to the other models of APROS in several ways. The solutions of other thermal hydraulic models can be given as boundary conditions to the model. Heat transfer is calculated between the flow model and the heat conduction model. The pump and valve models give input to the two-phase model and use the two-phase solution as their own input.

As an example of the two-phase flow validation some calculated experimental cases in four different test facilities have been shown.

The six-equation model has been used from 1992 in numerous power plant applications. Since that the further developing and testing has continuously been going on and the model has been validated against several separate and integral test facilities.

References

1. Siikonen, T., Numerical Method for One-dimensional Two-phase Flow. Numerical Heat Transfer 12(1987), pp. 1–18.

2. Wallis, G.B., One-dimensional Two-phase Flow. New York, N.Y. 1969. xxi + 408 p.

3. Properties of Water and Steam in SI-Units. Ed. by Schmidt, E. & Grigull, U. 3. ed. Berlin 1982. 194 p.

4. Bestion, D., The physical closure laws in the CATHARE code. Nuclear Engineering and Design 124(1990)3, pp. 229–245.

5. Wallis, G.B., Phenomena of Liquid Transfer in Two-phase Dispersed Annular Flow. International Journal of Heat and Mass Transfer 11(1968), pp. 783–785.

6. Bestion, D., Recent Developments on Interfacial Friction Models. European Two Phase Flow Group Meeting. Varese, May 21–24, 1990.

7. Lee, K. and Ryley, D.J., The Evaporation of Water Droplets in Superheated Steam. Journal of Heat Transfer 90(1968)4, pp. 445–451.

8. Maciaszek, T., Micaelli, J.C. and Bestion, D., Modélisation de l'autovaporisation dans le cadre d'un modèle à deux fluides. La Houille Blanche 1988:2, pp. 129–133.

9. Shah, M.M., A General Correlation for Heat Transfer during Film Condensation Inside Pipes. International Journal of Heat and Mass Transfer 22(1979)4, pp. 547–556.

10. Heat Transfer Correlations in Nuclear Reactor Safety Calculations, Vol. I. Publ. Nordic liaison committee for atomic energy. Stockholm 1985. 70 p.

11. Deruaz, R. and Petitpain, B., Modeling of Heat Transfer by Radiation during the Reflooding Phase of LWR. Proceedings of Specialist Meeting on the Behaviour of Water Reactor Fuel Elements under Accident Conditions. Spåtind, Norway, September 13–16, 1976. Arr. Committee on the Safety of Nuclear Installations, OECD Nuclear Energy Agency and Institutt for atomenergi, Norway.

12. Groeneveld, D.C. and Snoek, C.W., A Comprehensive Examination of Heat Transfer Correlations Suitable for Reactor Safety Analysis. Multiphase Science and Technology, Volume 2, 1986, pp. 181–274.

13. Clement, P. and Regnier, P., Heat Transfer Modelling at the Quench Front during Reflooding Phase of a LOCA (Interpretation of Experimental Results). Meeting of the European Two Phase Flow Group. Stockholm, May 29 – June 1, 1978.

14. Edwards, A.R. and O'Brien, T.P., Studies of phenomena connected with the depressurization of water reactors. Journal of the British Nuclear Society 9(1970)2, pp. 125–135.

15. Siikonen, T. and Kantee, H., Mixture Level Simulation Using RELAP5/MOD1. First Proceedings of Nuclear Thermal Hydraulics 1983 Winter Meeting. Publ. American Nuclear Society. 1983. Pp. 281–285.

16. Deruaz, R. and Tellier, N., Comparison Report on OECD-CSNI LOCA Standard Problem n° 7. Idaho 1979. OECD-CSNI, Working Group on Emergency Core Cooling in Water Reactors, CSNI/Report n° 55. 17 p.

Series title, number and
report code of publication

VTT Research Notes
VTT-TIED-2443

Author(s)
Hänninen, Markku & Ylijoki, Jukka

Title

The one-dimensional separate two-phase flow model of APROS

Abstract

The publication describes the one-dimensional two-fluid model of the computer program APROS used for the simulation of nuclear and conventional power plants. The work is based on the technical report from 1992. The treatment of the non-condensable gas mass equation has been added. The test results have been updated, so that the results correspond to the present APROS version 5.08. The derivation of the model from the governing partial differential equations is shown in detail and the solution procedure is described. Correlations for interfacial and wall friction and for heat transfer have been used to close the set of the linear equations. The friction and heat transfer packages of the model are documented. Finally, results of test cases calculated with the present model are briefly discussed.

ISBN

978-951-38-7224-3 (soft back ed.)
978-951-38-7225-0 (URL: http://www.vtt.fi/publications/index.jsp)

Series title and ISSN	Project number
VTT Tiedotteita – Research Notes 1235-0605 (soft back ed.) 1455-0865 (URL: http://www.vtt.fi/publications/index.jsp)	25524

Date	Language	Pages
August 2008	English	61 p.

Name of project	Commissioned by
	Fortum Nuclear Services Ltd., VTT Technical Research Centre of Finland

Keywords	Publisher
thermal-hydraulics, two-phase flow, one-dimensional flow, heat transfer, boron concentration, non-condensable gas	VTT Technical Research Centre of Finland P.O.Box 1000, FI-02044 VTT, Finland Phone internat. +358 20 722 111 Fax +358 20 722 4374

VTT Tiedotteita – Research Notes

2422 Vestola, Elina & Mroueh, Ulla-Maija. Sulfaatinpelkistyksen hyödyntäminen happamien kaivosvesien käsittelyssä. Opas louhoskäsittelyn hallintaan. 2008. 58 s. + liitt. 13 s.

2424 Ilomäki, Sanna-Kaisa, Simons, Magnus & Liukko Timo. Kohti yritysten vuorovaikutteista kehitystoimintaa. 2008. 45 s.

2425 Talja, Asko, Vepsä, Ari, Kurkela, Juha & Halonen, Matti. Rakennukseen siirtyvän liikennetärinän arviointi. 2008. 95 s. + liitt. 69 s.

2426 Nylund, Nils-Olof, Aakko-Saksa, Päivi & Sipilä, Kai. Status and outlook for biofuels, other alternative fuels and new vehicles. 2008. 161 p. + app. 6 p.

2427 Paiho, Satu, Ahlqvist, Toni, Piira, Kalevi, Porkka, Janne, Siltanen, Pekka & Tuomaala, Pekka. Tieto- ja viestintäteknologiaa hyödyntävän rakennetun ympäristön kehitysnäkymät. 2008. 60 s. + liitt. 34 s.

2430 Rinne, Tuomo, Tillander, Kati, Vaari, Jukka, Belloni, Kaisa & Paloposki, Tuomas. Asuntosprinklaus Suomessa. Vaikuttavuuden arviointi. 2008. 84 s.

2431 Nikkola, Juha, Mahlberg, Riitta, Siivinen, Jarmo, Pahkala, Anne, Lahtinen, Reima & Mahiout, Amar. Alumiinin pintaominaisuudet ja pintakäsittelyt. 2008. 49 s.

2432 Teknologiapolut 2050. Teknologian mahdollisuudet kasvihuonekaasupäästöjen syvien rajoittamistavoitteiden saavuttamiseksi Suomessa. Taustaraportti kansallisen ilmasto- ja energiastrategian laatimista varten. Ilkka Savolainen, Lassi Similä, Sanna Syri & Mikael Ohlström (toim.). 2008. 215 s.

2434 McKeough, Paterson & Kurkela, Esa. Process evaluations and design studies in the UCG project 2004–2007. 2008. 45 p.

2435 Salmela, Hannu, Toivonen, Sirra & Pekkala, Petri. Tapaustutkimus kuljetusrasituksista Trans-Siperian radalla. 2008. 59 s.

2436 Lindqvist, Ulf, Eiroma, Kim, Hakola, Liisa, Jussila, Salme, Kaljunen, Timo, Moilanen, Pertti, Rusko, Elina, Siivonen, Timo & Välkkynen, Pasi. Technical innovations and business from printed functionality. 2008. 73 p. + app. 6 p.

2437 Tiusanen, Risto, Hietikko, Marita, Alanen, Jarmo, Pátkai, Nina & Venho, Outi. System Safety Concept for Machinery Systems. 2008. 53 p.

2438 Koponen, Pekka, Pykälä, Marja-Leena & Sipilä, Kari. Mittaustietojen tarpeet ja saatavuus rakennuskannan automaattisten energia-analyysien näkökulmasta. 2008. 62 s. + liitt. 3 s.

2439 Mobile TV should be more than a television. The final report of Podracing project. Ed. by Ville Ollikainen. 2008. 71 p. + app. 4 p.

2442 Operational decision making in the process industry. Multidisciplinary approach. Ed. by Teemu Mätäsniemi. 2008. 133 p. + app. 5 p.

2443 Hänninen, Markku & Ylijoki, Jukka. The one-dimensional separate two-phase flow model of APROS. 2008. 61 p.

Julkaisu on saatavana	Publikationen distribueras av	This publication is available from
VTT PL 1000 02044 VTT Puh. 020 722 4520 http://www.vtt.fi	VTT PB 1000 02044 VTT Tel. 020 722 4520 http://www.vtt.fi	VTT P.O. Box 1000 FI-02044 VTT, Finland Phone internat. + 358 20 722 4520 http://www.vtt.fi

ISBN 978-951-38-7224-3 (soft back ed.) ISBN 978-951-38-7225-0 (URL: http://www.vtt.fi/publications/index.jsp)
ISSN 1235-0605 (soft back ed.) ISSN 1455-0865 (URL: http://www.vtt.fi/publications/index.jsp)